RNA splicing analysis deciphers developmental hierarchies and reveals therapeutic targets in adult glioma

Xiao Song, … , Bo Hu, Shi-Yuan Cheng

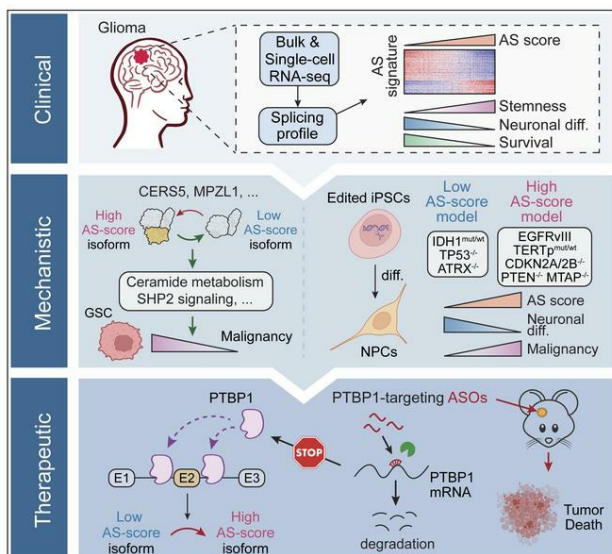**Research** In-Press Preview Cell biology Oncology

Graphical abstract

RNA Splicing Analysis Deciphers Developmental Hierarchies and Reveals Therapeutic Targets in Adult Glioma

Xiao Song[1], Deanna Tiek[1], Shunichiro Miki[2,#], Tianzhi Huang[1,##], Minghui Lu[1,###], Anshika Goenka[1,####], Rebeca Iglesia[1], Xiaozhou Yu[1], Runxin Wu[1], Maya Walker[1], Chang Zeng[3], Hardik Shah[4], Shao Huan Samuel Weng[5], Allen Huff[5], Wei Zhang[3], Tomoyuki Koga[6], Christopher Hubert[7], Craig M. Horbinski[8], Frank F. Furnari[2], Bo Hu[1*], and Shi-Yuan Cheng[1*]

[1]The Ken & Ruth Davee Department of Neurology, The Lou and Jean Malnati Brain Tumor Institute, The Robert H. Lurie Comprehensive Cancer Center, Simpson Querrey Institute for Epigenetics, Northwestern University Feinberg School of Medicine, Chicago, IL 60611, USA

[2]Department of Medicine, Division of Regenerative Medicine, Sanford Stem Cell Institute, University of California-San Diego, La Jolla CA 92093, USA

[3]Department of Preventive Medicine, The Robert H. Lurie Comprehensive Cancer Center, Simpson Querrey Institute for Epigenetics, Northwestern University Feinberg School of Medicine, Chicago, IL 60611, USA

[4]Metabolomics Platform, Comprehensive Cancer Center, The University of Chicago, Chicago, IL 60637, USA

[5]Proteomics Platform, Office of Shared Research Facilities, Biological Sciences Division, The University of Chicago, Chicago, IL 60637, USA

[6]Department of Neurosurgery, The University of Minnesota, Minneapolis, MN 55455, USA.

1 [7]Department of Biochemistry, School of Medicine, Case Western Reserved University,

2 Cleveland, OH, 44106, USA

3 [8]Departments of Pathology and Neurological Surgery, The Lou and Jean Malnati Brain

4 Tumor Institute, The Robert H. Lurie Comprehensive Cancer Center, Northwestern

5 University Feinberg School of Medicine, Chicago, IL 60611, USA

6 [#]Current address:

7 [#]Department of Neurosurgery, Institute of Medicine, University of Tsukuba, 1-1-1,

8 Tennodai, Tsukuba, Ibaraki, 305-8575, Japan

9 [##]State Key Laboratory of Cellular Stress Biology, Department of Cell Biology, School of

10 Life Sciences, Xiamen University, Xiamen 361102, Fujian, China

11 [###]Department of Neurology, Icahn School of Medicine at Mount Sinai, New York, NY

12 10029, USA

13 [####]Department of Hematology and Medical Oncology, Winship Cancer Institute, Emory

14 University, Atlanta, GA 30322, USA

15 *Correspondence

16 Shi-Yuan Cheng:

17 Address: 303 E. Superior St, Lurie 6-119, Chicago, IL 60611, US

18 Phone: (312)503-3043

19 E-mail: shiyuan.cheng@northwestern.edu; shiyuancheng@gmail.com

20 Bo Hu:

21 Address: 303 E. Superior St, Lurie 6-105, Chicago, IL 60611, US

22 Phone: (312)503-1031

23 Email: bo.hu@northwestern.edu

1 **ABSTRACT**

2 Widespread alterations in RNA alternative splicing (AS) have been identified in adult

3 gliomas. However, their regulatory mechanism, biological significance, and therapeutic

4 potential remain largely elusive. Here, using a computational approach with both bulk and

5 single cell RNA-sequencing, we uncover a prognostic AS signature linked with neural

6 developmental hierarchies. Using advanced iPSC glioma models driven by glioma driver

7 mutations, we show that this AS signature could be enhanced by EGFRvIII and inhibited

8 by in situ *IDH1* mutation. Functional validation of two isoform switching events in *CERS5*

9 and *MPZL1* shows regulations of sphingolipid metabolism and SHP2 signaling,

10 respectively. Analysis of upstream RNA binding proteins reveals PTBP1 as a key

11 regulator of the AS signature where targeting of PTBP1 suppresses tumor growth and

12 promotes the expression of a neuron marker TUJ1 in glioma stem-like cells. Overall, our

13 data highlights the role of AS in impacting glioma malignance and heterogeneity and its

14 potential as a therapeutic vulnerability for treating adult gliomas.

3

1   **INTRODUCTION**

2

3   Tumor heterogeneity is a hallmark of glioma and represents one of the major challenges

4   underlying therapeutic failure (1). The genetic heterogeneity of adult glioma have been

5   incorporated into a refined classification system, as per the 2021 WHO classification of

6   tumors of the central nervous system, which delineates glioma into three subtypes:

7   isocitrate dehydrogenase (IDH)-wildtype (WT) glioblastoma (GBM), astrocytoma with IDH

8   mutation (mut), and oligodendroglioma with IDH mut and 1p/19q-codeletion (2). In

9   addition to the diverse genetic and epigenetic alterations that drive heterogeneous

10   oncogenic programs in glioma (3), glioma cells also recapitulate multiple

11   neurodevelopmental and lineage differentiation programs, namely "cellular hierarchies",

12   driving another layer of heterogeneity (4). It has been proposed that IDH-mut gliomas are

13   comprised of three main subpopulations: stem/progenitor-like cells, oligodendrocytes-like

14   (OC-like) and astrocytes-like (AC-like) cells (5, 6). In IDH-WT GBM, the intra-tumoral

15   heterogeneity is represented by four interconvertible cellular states including neural-

16   progenitor-like (NPC-like), oligodendrocyte-progenitor-like (OPC-like), AC-like, and

17   mesenchymal-like (MES-like) states (7). Although there has been significant progress in

18   understanding inter- and intra-tumoral heterogeneity in gliomas, there are still challenges

19   in leveraging this knowledge to develop effective therapies.

20

21   RNA alternative splicing (AS) is a critical mechanism that generates multiple transcripts

22   from a single gene, thereby expanding diversities of the transcriptome (8). With a cell-,

23   tissue-, or developmental-specific regulation, AS is particularly common and conserved

4

in the mammalian nervous system and contributes to the functional complexity during brain development (9). Several AS-based signatures have been identified in glioma or GBM that showed association with patient prognosis, tumor recurrence, or immune microenvironment remodeling (10-12). A multi-omics study in GBM by the Clinical Proteomic Tumor Analysis Consortium (CPTAC) reported that the RNA transcript, protein, and phosphorylated protein abundances of genes related to mRNA splicing were upregulated in the classical subtype of GBM, indicating increased RNA splicing activities in a subset of GBM (13). However, our understanding of the relationship between dysregulated AS, tumor heterogeneity, and cellular hierarchies in glioma remains limited. The biological functions of most protein isoforms generated from glioma-associated AS alterations remain unknown, and there are significant gaps regarding how to target dysregulated AS to treat gliomas.

Here, we use bulk and single-cell RNA-seq data to determine the influence of dysregulated AS on tumor heterogeneity of adult gliomas and identify a prognostic AS signature associated with the neural developmental hierarchies in GBM and IDH-mut gliomas. We further show that this AS signature can be regulated by mutant EGFR or IDH1 and elucidate the functional mechanisms of AS events in genes *CERS5* and *MPZL1* in promoting glioma malignancy. Lastly, we investigate the involved upstream RNA-binding proteins (RBPs) and identify PTBP1 as a promising therapeutic target to dampen the malignant AS signature while promoting neuronal-like differentiation in glioma cells.

1 **RESULTS**

2

3 **Unsupervised splicing analysis in bulk glioma reveals a prognostic AS signature**

4 **linked to neural lineage differentiation.**

5 To decipher dysregulated AS in glioma heterogeneity, we compiled three bulk glioma

6 RNA-seq datasets, TCGA, CGGA (14), and our previously deposited Northwestern

7 University (NU) glioma dataset (15), and quantified Percent Spliced In (PSI) value for

8 each annotated event using MISO software (16) (Figure 1A and Supplemental Table 1-

9 4). We removed samples with poor sequence quality or that were originally assigned as

10 the "neural" subtype, for potential normal brain contamination (17), and filtered the data

11 to 1,300 AS events with consistent PSI variability across the three platforms

12 (Supplemental Figure 1A and 1B). Then, we performed unsupervised k-means

13 consensus clustering in filtered TCGA samples and identified two clusters that

14 significantly correlated with patients' prognosis (Supplemental Figure 1C-E). To identify

15 the most important AS events affecting the clustering, we built a random forest model (18)

16 with the 400 most representative samples, which were identified based on their positive

17 silhouette width, which is a measure of how well a sample is clustered (Supplemental

18 Figure 1F). We selected the top 200 AS events (affecting 170 genes) based on the Mean

19 Decrease Gini (MDG) value, a metric to quantify the importance of each feature in the

20 random forest model, and visualized the splicing pattern of these 200 events across the

21 three datasets, which revealed a continuum rather than a bimodal distribution (Figure 1B,

22 Supplemental Figure 1G, 1H, and Table 5). We further developed an AS score based on

23 the PSI values of the top 40 events (affecting 36 genes) with highest MDG values among

1   these 200 events (Supplemental Figure 1I and Method). In all three datasets, the splicing

2   pattern of the 200 events as well as the AS scores were significantly associated with

3   updated 2021 WHO tumor grades, *IDH1* mutation status, and the predefined molecular

4   subtyping (Figure 1B and 1C). Moreover, a higher AS score was associated with worse

5   overall survival in patients in both TCGA and CGGA datasets (Figure 1D and

6   Supplemental Figure 1J). Multivariable survival analyses using a Cox regression model

7   showed that our AS score system is an independent prognostic factor for glioma patient

8   survival after controlling for the 2021 WHO classification, gender, age, *IDH* mutation,

9   1p/19q co-deletion, and genetic alterations in *EGFR* and *TP53* (Figure 1E and

10 Supplemental Figure 1K). Intriguingly, the AS score is significantly associated with the

11 expression of specific neural lineage markers, showing a positive correlation with markers

12 of neuroepithelial cells and radial glia, but a negative correlation with markers of

13 differentiated lineages, like neuronal lineages (Figure 1F), suggesting a connection

14 between AS and the developmental hierarchy of gliomas.

15

16 As an orthogonal validation of splicing estimation, we performed AS analysis in TCGA

17 samples using rMATS (19). A high concordance in PSI prediction among the 200 AS

18 events was observed between the results from MISO and rMATS algorithms

19 (Supplemental Figure 1L and 1M), supporting the rigor of our AS analysis.

20

21 Among the 200 events, skipped exons (SE) and mutually exclusive exons (MXE) were

22 the predominant AS types (Figure 2A). 123 events were annotated in a functional impact

23 database for human AS events (20) that could potentially affect isoform

1   function/expression, including alterations in posttranslational modification, protein domain,

2   or induction of nonsense-mediated decay (Figure 2B). The 200 events affect 170 genes

3   enriched for biological processes related to neuron differentiation and function (Figure

4   2C), and 139 genes showed no significant change in their total transcript levels between

5   tumors with high or low AS scores (Figure 2D), suggesting that their functions are

6   regulated at the AS level. Moreover, the differences in AS landscapes between AS score-

7   high and -low gliomas is comparable to the AS switch observed in a neuronal

8   differentiation model from human embryonic stem cell (ESC) (21), further supporting the

9   linkage of this AS signature with neuronal lineage differentiation (Figure 2E and 1B). As

10   expected, the AS score of normal adult brain was found to be markedly lower than those

11   of glioma (Figure 2F, 2G, and Supplemental Figure 2A). Although no significant difference

12   in AS score between bulk fetal and adult brain tissues (22) were observed (Supplemental

13   Figure 2B), single-cell (sc) RNA-seq profiles (23) revealed a lower AS score in neurons

14   and oligodendrocytes compared to astrocytes from adult brains, while the quiescent

15   neurons exhibited a lower AS score compared to the replicating neuronal progenitors from

16   fetal brains (Figure 2H).

17

18   For each event, we designated the isoform associated with a low AS score as isoform 1

19   (iso1), and the isoform associated with a high AS score as isoform 2 (iso2). Interestingly,

20   in seven events whose biological impact has been previously reported (24-30), either the

21   iso1 inhibits tumor growth or iso2 promotes tumorigenicity (Figure 2I and Supplemental

22   Figure 2C). To validate our AS analysis, we selected ten events, including five events

23   with known isoform-specific functions (USP5, TPM1, PKM, NED1, and FYN) and five

1 events (MPZL1, CARM1, ATG13, FEZ2, and CERS5), whose isoform-specific functions

2 in cancer are less-studied but occur in genes implicated in critical cancer-related

3 processes (Figure 2I). We observed AS changes in these ten genes across the normal

4 brains, low AS score gliomas, and high AS score GBMs, validating our bioinformatic

5 analyses with significant correlations between MISO-estimated PSI and PCR-quantified

6 PSI (Figure 2J). We also detected these events in GBM stem-like cells (GSC) 1478,

7 GSC1485, the GBM line U87, and normal human neural progenitors (NHNPs; Figure 2I).

8 NHNPs express more iso1 and less iso2 than GSC/GBM lines in most detected events.

9 In addition, those ten events were alternatively spliced during ESC-neuronal

10 differentiation and all of them were significantly associated with patient outcomes

11 (Supplemental Figure 2D).

12

13 **Intra-tumoral AS heterogeneity is associated with developmental hierarchy in**

14 **glioma.**

15 To investigate how the AS signature that we defined from bulk gliomas also contributes

16 to the intra-tumoral heterogeneity in glioma, we analyzed published full-length scRNA-

17 seq data from 7 IDH-WT GBM and 7 IDH-mut glioma patients (31). To increase the read

18 coverage for AS estimation, we integrated cells from the same cellular state within each

19 patient as a pseudo-bulk before AS profiling (Figure 3A and Supplemental Figure 3A).

20 The mesenchymal (MES) state has been subdivided into two categories: hypoxia-

21 independent MES.1 and hypoxia-dependent MES.2. Similarly, the neural progenitor cell

22 (NPC) module has been further divided into two groups: NPC.1, which expresses

23 oligodendrocyte progenitor cell (OPC)-related genes, and NPC.2, which expresses genes

1 related to neuronal lineage (31). The number of detected events significantly increased

2 by utilizing this pseudo-bulk strategy compared to analysis at single-cell resolution

3 (Supplemental Figure 3B). Then we performed a hierarchical clustering analysis with the

4 PSI data of detected events from our 200-event list in each cell state-based pseudo-bulk

5 (Figure 3B). Most of the cellular states between IDH-WT and -mut tumors were separated

6 from each other and showed similarity with the AS landscapes observed in TCGA bulk

7 RNA-seq data. Surprisingly, the NPC.2 pseudo-bulks from IDH-WT tumors clustered

8 together with the stem-like pseudo-bulks from IDH-mut tumors, displaying similar AS

9 patterns in genes like *CERS5* and *PKM*, as well as a comparably low AS score (Figure

10 3B). Gene expression analysis of neuronal lineage markers demonstrated that most

11 IDH1-WT cells expressed high levels of stem/progenitor or astrocyte markers, except for

12 NPC.2, which expressed immature neuron markers, similar to the IDH1-mut stem-like

13 subpopulations (Figure 3C), further supporting the link between neuronal differentiation

14 and our AS signature.

15

16 The AS score was relatively lower in all cell states from IDH-mut vs IDH-WT tumors

17 (Figure 3D). However, when focusing on specific events, they exhibited a heterogeneous

18 splicing pattern across different cellular states (Figure 3D and Supplemental Figure 3C).

19 For instance, NPC.2 cells of IDH-WT tumors and stem-like cells of IDH-mut tumors

20 exhibited a similar splicing pattern in genes *PKM*, *NRCAM*, and *PICALM*, which differed

21 from the splicing pattern observed in other cellular states. IDH-WT MES cells exhibited

22 differential AS of *MAP4K4*, while IDH-mut OC-like cells exhibited differential AS of *TPM3*.

1   Overall, our AS signature not only contributes to the intra-tumoral heterogeneity but is

2   also linked to developmental hierarchies within each gliomas.

3

4   **Glioma driver mutations modulate AS landscape and neural developmental**

5   **programs.**

6   Considering the association between AS signature and *IDH* mutation status (Figure 1B),

7   we speculated that genetics might play a role in shaping the heterogeneous AS landscape.

8   By analyzing TCGA data, we identified three genotypes that exhibited increasing AS

9   scores: 1) *IDH1*-mut + *TERT* promoter (*TERT*p)-mut + 1p/19q co-del + *CIC*/*FUBP1*-mut;

10   2) *IDH1*-mut + *TP53*-mut + *ATRX*-mut; 3) *TERT*p-mut, *CDKN2A*/*CDKN2B*/*MTAP-del*,

11   *EGFR*-amp/mut + *PTEN*-mut data (Figure 4A and Supplemental Figure 4A). To assess

12   the impact of these genetic alternations on the AS landscape, we utilized a human iPSC-

13   derived glioma "avatar" model (32, 33). Given the difficulty of modeling 1p/19q co-deletion,

14   we focused on the latter two genotypes. Using CRISPR/Cas9, we developed edited

15   human iPSCs harboring $TP53^{-/-}$, $IDH1^{R132H/WT}$, $ATRX^{-/-}$ (T, I, A), or $PTEN^{-/-}$, $CDKN2A/2B^{-}$

16   $^{/-}$, $TERTp^{C228T/WT}$, EGFRvIII-overexpression (OE), plus $MTAP^{-/-}$ (P, C, T, E, M; Figure 4B-

17   D and Supplemental Figure 4B). Edited iPSCs were then differentiated into neural

18   progenitor cells (NPCs) (33). The differentiation status was confirmed by the

19   downregulation of pluripotency markers and upregulation of NPC markers in all edited

20   NPCs except for iPSC^{PCTE}-NPC and iPSC^{PCTME}-NPC, which failed to induce *PAX6*

21   expression (Supplemental Figure 4C). Considering that the EGFRvIII-OE in iPSCs might

22   influence *PAX6* expression during NPC induction, we generated two other NPCs,

23   iPSC^{PCT}-NPC^E and iPSC^{PCTM}-NPC^E, in which the EGFRvIII was overexpressed at the

1   NPC stage, and the *PAX6* expression was significantly upregulated (Supplemental Figure

2   4C-E). We characterized these two edited NPCs as "PCTE" and "PCTME" models.

3

4   The edited NPCs representing each of the eight genotypes (IDH1-mut: T, TI, TA, TIA;

5   IDH1-WT: PCT, PCTM, PCTE, PCTME) were assessed for their cellular properties.

6   Compared to other edited NPCs, PCTE and PCTME displayed an increased capacity for

7   proliferation and self-renewal (Figure 4E and 4F), validating the established oncogenic

8   function of EGFRvIII. Next, we evaluated the AS landscape in these edited NPCs by using

9   a 3D organoid model to recapitulate the composition and architecture of primary gliomas

10 (Supplemental Figure 4F) (34). We performed transcriptome analysis on those organoids

11 and focused on our 200-event AS landscape. Intriguingly, we observed that *IDH1*

12 mutation had a modest impact on the AS profile, shifting it towards a lower AS score,

13 whereas EGFRvIII significantly drove an AS signature with an increased score (Figure

14 4G and Supplemental Figure 4G). Consistently, *IDH1* mutation induced higher expression

15 of neuronal lineage markers, while EGFRvIII blocked the differentiation of all three

16 lineages, keeping cells in a stem/progenitor stage (Figure 4G).

17

18 Consistent with the in vitro behaviors, NPC PCTE and PCTME xenografts grew faster

19 and shortened mouse survival compared to TI and TIA tumors (Figure 5A, 5B, and

20 Supplemental Figure 4H). H&E and immunostaining for human-specific LaminB2

21 confirmed tumor formation in all groups (Figure 5C). Xenograft transcriptome analysis

22 confirmed the differential AS profiles between mutant *IDH1*-driven and EGFRvIII-driven

23 tumors, which recapitulated the clinical AS landscape (Figure 5D-F). Additionally, all

1   TI/TIA xenografts were assigned to the "proneural" subtype, while PCTE/PCTME

2   xenografts were either in the "classical" or "mesenchymal" subtype (Figure 5G). Genes

3   with elevated expression in PCTE/PCTME tumors compared to TI/TIA tumors were

4   enriched for biological processes related to cell division, while genes upregulated in

5   TI/TIA tumors were involved in neuronal function (Figure 5H). This analysis indicated that

6   the iPSC-based model of gliomas displayed distinct mutation-dependent variation in their

7   transcriptome, which recapitulated the gene expression and AS signatures of clinical

8   gliomas.

9

10   To investigate whether mutant EGFR could drive AS changes in the *IDH1*-mut genetic

11   background, we overexpressed EGFRvIII in the TIA model. Our findings revealed that

12   EGFRvIII substantially enhanced cell proliferation and induced AS changes in the *IDH1*-

13   mut background, similar to its effects observed in the PCT background (Supplemental

14   Figure 4I-K). Nevertheless, the introduction of the *IDH1*-R132H mutation into *IDH1*-WT

15   GSC1478 cells did not induce AS changes in detected genes and exhibited no impact on

16   cell proliferation or in vivo tumorigenesis (Supplemental Figure 4L-Q). These data

17   highlighted the regulatory role of EGFRvIII in global AS across different glioma models;

18   In contrast, the impact of *IDH1* mutation on the AS landscape appears to be dependent

19   on the specific genetic background.

20

21   **AS of CERS5 and MPZL1 influences the oncogenic potential of glioma cells.**

22   To investigate the biological relevance of the AS signature we identified, we first assessed

23   the exon skipping event in *CERS5* exon 10 (E10). Ceramide, the building block of all

sphingolipids and a bioactive intermediate in signal transduction, is synthesized by a family of six ceramide synthases, CERS1-6, where each generate ceramides with specific N-acyl chain lengths (35). Previous reports indicate chain length-dependent function of ceramides in tumor growth and apoptosis (36). From CPTAC lipidome data (13), we found a significant alteration in the abundance of ceramides with distinct chain lengths (Figure 6A and Supplemental Figure 5A). Specifically, C16-ceramide was identified as the most highly upregulated species in GBM compared to normal brains (Figure 6B). C16-ceramide is synthesized by CERS5 and CERS6, but the overall expression change of these two genes could not fully explain the upregulation of C16-ceramide in GBM (Figure 6C and Supplemental Figure 5B). Instead, E10 of *CERS5* is alternatively spliced between GBM and normal brains and the PSI of *CERS5*-E10 is significantly correlated with C16-ceramide abundance (Figure 6D and Supplemental Figure 5C), indicating an isoform-specific function of CERS5 in increasing the levels of C16-ceramide in GBM.

CERS5 is an ER membrane protein consisting of five predicted transmembrane segments. The AS of *CERS5*-E10, a non-triplet exon whose inclusion causes a frameshift and an alternative stop code in the last exon (E11), generates two isoforms with distinct cytosolic C-termini (Figure 6E). With the CPTAC proteomic data, we confirmed that normal brain preferentially expresses the isoform including E10 (iso1), while GBM preferentially expresses the isoform lacking E10 (iso2; Figure 6F), which contains four serine phosphorylation sites encoded by E11 (Figure 6E and Supplemental Figure 5D). Phosphorylation at these four serine sites is required for the increased C16-ceramide level after CERS5 overexpression (37). As expected, we detected serine phosphorylation

14

1   of exogenously expressed CERS5 iso2, but not in iso1, in GSCs (Figure 6G). To study

2   the isoform-specific function, we knocked out (KO) CERS5 in GSCs, in which iso2 is the

3   dominant isoform (Figure 2I), then overexpressed either iso1 or iso2 in the KO cells

4   (Supplemental Figure 5E-G). Ablation of CERS5 resulted in a significant reduction of C14

5   and C16-ceramides, which could be rescued by re-expression of iso2, but not iso1 (Figure

6   6H and Supplemental Figure 5H). Furthermore, CERS5 KO inhibited GSC cell

7   proliferation, sphere-forming frequency, and suppressed brain xenograft growth,

8   extending animal survival. Re-expression of CERS5 iso2, but not iso1, rescued the

9   inhibition by CERS5 KO on GSC tumorigenicity (Figure 6I-L, Supplemental Figure 5I, and

10   5J).

11

12   To further investigate AS signature event, we developed a CRISPR-based AS

13   manipulation method to screen functional events (Figure 7A) (27). We selected eight AS

14   candidates based on their importance scores calculated from the random forest model as

15   well as CRISPR targeting feasibility of their splice sites (Supplemental Figure 5D) and

16   successfully induced the exon skipping in six candidates, confirmed by sanger

17   sequencing (Figure 7B and Supplemental Figure 5K). We showed that the induced exon

18   skipping of *TPM1*-E6, *MPZL1*-E5, or *CSNK1D*-E9 significantly inhibited GSC1485 cell

19   viability. Of note, the induced skipping of *MPZL1*-E5 inhibited in vitro cell proliferation as

20   well as in vivo tumorigenesis in GSC1478 (Figure 7C-E). However, normal NHAs and

21   NHNPs do not require *MPZL1*-E5 inclusion for their viability (Figure 7C and Supplemental

22   Figure 5L). MPZL1 was identified as a binding protein of tyrosine phosphatase SHP2 and

23   has been demonstrated to be upregulated in various cancers and promote cell

15

1   proliferation and migration (38-40). Compared with the E5-excluded iso1, the E5-included

2   iso2 contains an extended C-terminus that harbors two tyrosine (Y) residues, Y241 and

3   Y263 (Figure 7F). Phosphorylation at Y241 and Y263 of MPZL1 was shown to mediate

4   its interaction with SHP2 (41). We confirmed that only iso2 but not iso1 could bind to

5   SHP2 in GSCs (Figure 7G and Supplemental Figure 5M). SHP2 regulates key oncogenic

6   pathways, including RAS-MAPK and PI3K-AKT, downstream of several receptor tyrosine

7   kinases (42). Indeed, phosphorylation of AKT (p-AKT) and p-ERK were decreased in

8   MPZL1 KO GSC1485 cells compared with control cells, whereas re-expression of

9   exogenous MPZL1 iso2, but not iso1, in MPZL1-KO cells enhanced both p-AKT and p-

10   ERK (Figure 7H). Furthermore, the exogenous expression of iso2, but not iso1, rescued

11   the MPZL1 KO-impaired cell growth in GSCs (Figure 7I).

12

13   **A group of RBPs modulate the AS landscape in glioma.**

14   To identify the upstream regulator(s) of the identified AS signature, we analyzed the

15   sequence characteristics surrounding the splice sites of the 200 events. We focused on

16   the SE and MXE events, and segregated the exons into those that are more included in

17   GBM and those that are more excluded in GBM compared to normal brain. There was no

18   significant difference in the splice site strength between included and excluded exons

19   calculated with three different scoring models (Supplemental Figure 6A). However,

20   included exons had substantially lower GC content upstream of the 3' splice site (3'SS)

21   as compared with the excluded exons (Supplemental Figure 6B). Next, a de novo motif

22   analysis identified potential PTBP1-binding motifs enriched in both the upstream

23   (CYCUCY) and downstream (CUBCCY) intronic regions of the excluded exons, while a

potential serine and arginine-rich (SR) splicing factor (SRSF)3-binding motif (CYUCWKC) was found enriched in the exonic regions of the included exons (Figure 8A).

Next, we analyzed the gene expression of 276 splicing-regulating RBPs and identified 29 RBPs whose expression correlated with the AS score in all three glioma datasets (Figure 8B). The differential expression of PTBP1, SNRPB, SNRPD2, and SRSF3 was corroborated at the protein level in NU tissue samples and GBM cell lines (Figure 8C). Consistently, these AS score-correlated RBPs are also differentially expressed between mutant IDH1- and EGFRvIII-driven iPSC glioma models (Figure 8B, 8D, Supplemental Figure 6C-E). Of interest, these RBPs exhibit distinct expression patterns during the neuronal differentiation process. Most of the positively correlated RBPs, including PTBP1, gradually decrease their expression during neuronal differentiation, while some of the negatively correlated RBPs, including RBFOX1, show increasing expression (Figure 8B). Splicing analysis in cells affected by PTBP1-KO, RBFOX1-overexpression (OE), or SRSF3-KO (27, 43, 44) revealed that each of these three RBPs regulated a subset of the 200 events (Figure 8E, Supplemental Figure 6F, and Table 6). This observation was validated by RT-PCR in GSCs (Figure 8E).

Furthermore, we investigated the expression of these 29 RBPs and their association with AS landscape at the single-cell level (31). In line with the findings from the bulk RNA-seq analysis, a hierarchical clustering analysis showed that most IDH-WT cells were distinguished from IDH-mut cells based on their elevated expression of AS-positively correlated RBPs, including PTBP1, SNRPB2, and SNRPD (Supplemental Figure 6G and

17

1   6H). As expected, the NPC.2 subpopulation of IDH-WT tumors clustered together with

2   IDH-mut cells, which is consistent with the finding from the AS-based clustering analysis

3   (Figure 3B). In contrast to the widespread expression of AS-positively correlated RBPs,

4   most of the negatively correlated RBPs displayed a scattered expression pattern, with

5   expression limited to a small subset of cells, predominantly IDH-mut. Additionally, we

6   observed significant correlations between certain RBPs and specific AS events at single-

7   cell resolution (Supplemental Figure 6I).

8

9   **Targeting PTBP1 inhibits cell growth and induces neuronal-like differentiation of**

10 **GSCs.**

11 Next, we determined the biological function of specific RBPs in glioma cells that were

12 positively or negatively correlated with AS scores. KO or KD of PTBP1, SRSF3, SNRPB,

13 or SNRPD2 significantly reduced the proliferation of GSC1485 cells, while OE of RBFOX1,

14 but not CELF4 or SRRM4, inhibited cell growth (Figure 9A and Supplemental Figure 7A).

15 Of interest, a mutual-regulatory network may exist in the expression among these RBPs,

16 wherein SRSF3-KO decreased PTBP1 expression, SNRPB-KD reduced SRSF3 and

17 SNRPD2 expression, and SNRPD2-KD led to the dephosphorylation of SRSF3

18 (Supplemental Figure 7B).

19

20 We focused on PTBP1 to further study its function in GSCs due to its strongest correlation

21 with the AS score (Figure 8B). KD of PTBP1 not only induced apoptosis and decreased

22 self-renewal in GSC1478 cells, but also induced a neuronal-like morphology and the

23 expression of a neuron marker TUJ1 under a neuronal differentiation culture condition

18

1 (Figure 9B, 9C and Supplemental Figure 7C), which further highlights the association

2 between RBP/AS networks and differentiation programs in glioma. Through the

3 modulation of *CERS5*-E10 AS (Figure 8E), PTBP1 KD led to a significant decrease of

4 C16-ceramides in GSC1478 (Supplemental Figure 7D).

5

6 We then assessed the therapeutic vulnerability of targeting PTBP1 in glioma by using an

7 antisense oligonucleotide (ASO)-based therapy (45). Compared to a control GFP-ASO,

8 the PTBP1-ASO1 decreased PTBP1 protein level and inhibited in vitro GSC growth but

9 had no effect on NHNPs or NHAs (Figure 9D). Notably, PTBP1 targeting exerted much

10 stronger anti-tumor effects in *IDH1*-WT iPSC-NPC than in *IDH1*-mut iPSC-NPC (Figure

11 9E and Supplemental Figure 7E). Consistently, PTBP1 KO had milder effects on the

12 *IDH1*-mut GSCs compared with *IDH1*-WT GSCs (Supplemental Figure 7F), indicating

13 variable dependence on PTBP1-modulated AS program in *IDH1*-WT and -mut tumors.

14

15 Next, we assessed the therapeutic effects of the PTBP1-ASO or a control-ASO through

16 intratumoral delivery in an orthotopic xenograft model of GSC1478 cells. Consistently,

17 PTBP1-ASO1 treatment significantly inhibited the growth of orthotopic tumor xenografts

18 and prolonged animal survival (Figure 9F-H). Further analysis of ASO-treated tumor

19 xenografts showed effective downregulation of PTBP1 expression and induction of

20 apoptosis in PTBP1-ASO group (Supplemental Figure 7G). Taken together, these results

21 suggest that PTBP1-targeting ASO produces a potent antitumor effect in the *IDH1*-WT

22 model.

DISCUSSION

Considerable progress has been made in uncovering dysregulated AS in adult glioma. Previous studies have been primarily focused on either identifying the AS signature related to glioma subtyping (46), prognosis (10, 47), or recurrence (11) using bulk RNA-seq data, or conducting functional investigations of specific splicing factors or AS events (12, 48, 49). While some subtyping or prognostic AS signatures have been identified (10, 46, 47), these studies often lack validation across multiple datasets and fail to explore the biological relevance behind the AS signatures. In contrast, our study provides the most comprehensive AS profiling to date in both IDH-WT and -mut adult gliomas through integrating multiple glioma datasets, followed by rigorous validation of the differential splicing patterns in clinical samples, GSCs, and iPSC-based glioma models. ScRNA-seq analysis not only validate our data on bulk RNA-seq but also reveals an intra-tumoral heterogeneity reflected at AS level. Moreover, our data reveal a link between the AS landscape and developmental hierarchies in glioma cells. Accumulating evidence revealed that while exhibiting considerable plasticity, gliomas follow a typical neurodevelopmental trajectory where multipotent cells differentiate into neurons, astrocytes, or oligodendrocytes (5-7). The identified AS signature is strongly associated with the multipotent state of gliomas and shows a negative correlation with neuronal lineage differentiation. Interestingly, the AS and RBP signatures in NPC.2 subpopulation in IDH-WT tumors share a similarity with IDH-mut tumors, especially the stem-like population. We speculate that the predefined stem-like subgroup in IDH-mut tumors is more neuronal lineage restricted rather than a multipotent population based on their

1   expression levels of lineage markers and lower AS scores. This may explain the reported

2   low rate of dedifferentiation from OC- or AC-like cells to stem-like cells in IDH-mut tumors

3   (31). The distinct AS landscapes observed between IDH-WT and IDH-mut gliomas that

4   link to neurodevelopmental programs suggest variations in the cell-of-origin for these two

5   glioma subtypes (50). In brief, with its cell-, tissue-, or developmental-specific regulation,

6   AS provides another perspective for studying the developmental hierarchy in gliomas.

7

8   While extensive AS alterations have been identified in cancers, the functional

9   investigation of these changes is often lacking. In this study, we provide mechanistic

10   insights into the isoform-specific functions in *CERS5* and *MPZL1*. CERS5 is known to be

11   responsible for C16-ceramide synthesis that is critical for sphingolipid signaling, tumor

12   growth, and cell apoptosis (35, 36). However, there has been no investigation into the

13   differential AS of CERS5 in cancers and its functional implications for tumorigenesis.

14   Here, we show that the AS of *CERS5* E10 is an important mechanism for the increased

15   C16-ceramide in GBM compared with normal brain. The GBM-associated CERS5 iso2,

16   which contains four phosphorylated serine residues at its cytoplasmic tail, is required for

17   the synthesis of C16-ceramide in GSCs. Moreover, CERS5 iso2 but not iso1 promotes

18   GSC growth and self-renewal capacity in vitro, and tumorigenicity in vivo. MPZL1 was

19   shown to interact with SHP2 and regulate downstream oncogenic signaling (38, 41). Our

20   data reveal the differential AS of *MZPL1* E5 in gliomas, showing a higher inclusion in AS

21   score-high gliomas compared to AS score-low gliomas and normal brains.

22   Mechanistically, E5+ isoform includes Y241 and Y263 in its C-terminal tail which was

23   reported to mediate the interaction between MPZL1 and SHP2 (41). Consistently, we

show that E5- isoform lost its interaction with SHP2 and only E5+ isoform could activate

AKT/ERK signaling and promote GSC proliferation. In conclusion, the AS isoforms from

the AS signature we defined here affect different hallmarks of cancer including

metabolism (PKM2) (25), Src-signaling (FYN) (29), mitosis (NDE1) (27), ceramide

synthesis (CERS5), and SHP2-signaling (MPZL1) – thereby contributing together to the

malignancy and heterogeneity of gliomas.

Our data reveal a link between the oncogenic mutations, neurodevelopmental program,

and AS heterogeneity in gliomas. With our hiPSC-derived glioma avatar system, we show

that glioma-driven mutations, *IDH1*-mut and EGFRvIII, not only affect the AS landscapes

and tumorigenicity, but also modulate the neural differentiation programs. Based on the

AS analysis and expression analysis of neural marker genes, we show that EGFRvIII

sustains the iPSC-derived NPCs in a multipotent state, while *IDH1*-mut promotes

differentiation towards neuronal lineage. Our observation that EGFRvIII impaired the

PAX6 induction during iPSC to NPC differentiation also suggests its roles in maintaining

stemness. In fact, EGFR signaling is well-known for its crucial role in neural stem cell pool

maintenance as well as the inhibition of neuronal differentiation (51, 52). Although *IDH1*-

mut was shown to block cell differentiation in tumors of different tissue origins (53, 54),

whether it hinders the differentiation of all three neural lineages in glioma remains

controversial. Here, we find that instead of blocking the differentiation of all neural

lineages, *IDH1*-mut shifted differentiation from glial to neuronal lineage. Our finding

contradicts two previous studies that demonstrated the inhibitory effect of *IDH1*-mut on

the expression of both astrocytic and neuronal markers (55, 56). The major difference

1 between our model and theirs is that they overexpressed exogenous mutant IDH1,

2 whereas we mutated the endogenous *IDH1* gene locus, thus recapitulating the clinical

3 heterozygous *IDH1* mutation. Moreover, our data corroborates a previous study showing

4 that *IDH1*-mut reduced the expression of GFAP and concomitantly increased the

5 expression of the neuronal lineage marker TUJ1/β3-Tubulin (54). Further investigations

6 are needed to determine how mutant IDH1 or EGFR regulate neural lineage

7 differentiation and what functional roles AS plays in this process. A plausible mechanism

8 linking genetic drivers and AS could involve the methylome change induced by *IDH1*-mut,

9 which may affect specific RBPs from binding their target pre-mRNA (57), or the EGFR-

10 activated AKT/SRPK pathway, which increases SR family protein phosphorylation (58).

11

12 Last, we identified two subsets of RBPs that positively or negatively correlate with the

13 malignant AS signature. Interestingly, these RBPs also exhibit distinct expression

14 patterns during neuron differentiation and correlate with AS landscapes in gliomas at the

15 single cell level. We also showed that PTBP1 and RBFOX1 displayed opposing effects

16 on the cell proliferation of *IDH1*-WT GSCs. Context-dependent RBP regulation was also

17 demonstrated when PTBP1 was depleted in *IDH1*-WT or -mut GSCs and iPSC-NPCs.

18 PTBP1 has been described as one of the key RBPs in regulating AS in neural

19 development and known oncogenic AS gene isoforms such as *PKM* and *USP5* in glioma

20 (24, 45, 48). Recent studies show that targeting PTBP1 by ASOs can convert midbrain

21 astrocytes to dopaminergic neurons and improved Parkinson's disease in mice (45), and

22 that PTBP1 knockdown promotes neuronal-like differentiation of IDH-WT glioblastoma

23 cell lines (59). Our data not only confirm PTBP1's role in regulating neuronal-like

1   differentiation in GSCs and but also unveil its previously unknown function in sphingolipid

2   metabolism/C16 ceramide synthesis through regulating *CERS5* E5 SE. Additionally, our

3   study demonstrates that in situ delivery of PTBP1-ASOs successfully inhibited the growth

4   of GSC tumor xenografts and prolonged survival in a mouse model. However, tumor

5   regrew with PTBP1-untargeted cells in the end due to inadequate diffusion of ASOs

6   throughout the entire tumor. Further investigation is necessary to improve the delivery

7   strategy for ASOs to ensure robust tumor targeting. Traditional therapies aim to target

8   tumor-specific features to eradicate specific populations but can induce cellular

9   reprogramming to evade treatment. This is particularly common in tumors with high

10   plasticity, including GBM. Therefore, therapeutics that restrain tumor plasticity, such as

11   differentiating tumor cells to a terminal stage, may be necessary for effective glioma

12   treatment (60). We propose that targeting the AS regulator PTBP1 and/or other key RBPs

13   that regulate AS landscapes represents a potential avenue for neuronal-like differentiation

14   therapy in glioma, particularly in GBMs.

1 **Methods**

2

3 **Sex as a Biological Variable**

4 Our study examined orthotopic glioma tumor xenografts in male and female animals, and

5 similar findings are reported for both sexes.

6

7 **AS Analysis in Bulk RNA-seq Datasets of Human Gliomas**

8 RNA-seq data from TCGA-LGG and -GBM datasets (530 low-grade gliomas, 169 GBMs,

9 and 5 normal brains) were downloaded from https://portal.gdc.cancer.gov/legacy-archive/.

10 Reads of TCGA-GBM datasets were trimmed to 48 bp from 3' ends, the same length as

11 TCGA-LGG datasets, to avoid the bias on AS analysis caused by read length variation.

12 RNA-seq data from CGGA database (14), including 182 LGGs and 143 GBMs, were

13 downloaded from http://cgga.org.cn. RNA-seq analysis was performed in clinical glioma

14 specimens from the Northwestern Nervous System Tumor Bank (NSTB, including 18

15 LGGs and 85 GBMs) and 15 normal brain tissue specimens from the NIH NeuroBiobank

16 as previously reported (15), referred as NU dataset. RNA-seq data from CPTAC database

17 (13), including 100 GBMs and 9 normal brains, were downloaded from PDC portal,

18 https://pdc.cancer.gov/pdc. All the reads from TCGA, CGGA, NU, and CPTAC datasets

19 were aligned to the human genome reference hg19 (genecode_v19) using HISAT2 v2.0.4

20 (61). The alignments were processed through the MISO v0.5.4 (16) or rMATS v4.0.2 (19)

21 to estimate the PSI (percentage spliced in, ranging from 0 to 1) value for each AS event.

22 Those samples that showed undetectable PSI values in more than 40% of total annotated

23 events (TCGA: 26/699; CGGA: 12/325; NU: 3/118) were filtered out to ensure high

1   sequence quality for AS analysis. Before performing clustering analysis based on the PSI

2   data of TCGA samples, several filtering criteria were applied to select informative and

3   reliable AS events based on the PSI values calculated by MISO (v0.5.4), including: 1)

4   Max(PSI)-Min(PSI) > 0.6; 2) SD(PSI) >0.1; 3) the range of 95% confidence intervals (CIs)

5   of the PSI estimates < 0.5 in more than 80% samples. A total of 1,300 AS events satisfied

6   these 3 criteria in TCGA, CGGA, and NU datasets. Samples with a "Neuronal" molecular

7   subtype were removed in consideration of potential normal brain contamination. We

8   performed   a   consensus   clustering   analysis   on   GenePattern   platform

9   (www.genepattern.org) using the following parameters: clustering algorithm-KMeans;

10   distance measure-Pearson; resampling iterations-1000; normalize type-AS event wise

11   and identified two clusters. Next, we built a random forest model (R-package:

12   randomForest, v4.6.14) with the top 400 representative samples selected based on their

13   silhouette width values (R-package: cluster v2.1.0). The 200 most important AS events

14   were selected representing the AS signature according to the Mean Decrease Gini value

15   generated by the random forest algorithm. The heatmap visualization of the 200-event

16   signature was conducted using the TreeView tool (v1.2.0). From these 200 events, we

17   further narrowed down to 40 events based on their PSI distribution and MDG values to

18   develop an AS score. The events were categorized into two groups according to their PSI

19   distribution among glioma samples: group 1 events show higher PSI values in samples

20   with worse survival; group 2 events show lower PSI values in samples with worse survival

21   (Supplemental Figure 1I). We selected the top 20 events with the highest MDG values in

22   each group to compose the final set of 40 events. We chose to use 40 events instead of

23   including all 200 events to calculate the AS score, taking into consideration their MDG

1 distribution as illustrated in Supplemental Figure 1G, which suggests that the top 40

2 events are the major contributors of the AS-based clustering in glioma. To calculate the

3 AS score, we subtracted the average PSI value of group 2 events from the average PSI

4 value of group 1 events. The functional prediction of AS events were performed on

5 ASpedia website (http://combio.snu.ac.kr/aspedia/) (20). The neural lineage markers list

6 is obtained from the neural marker booklet available on the Abcam website:

7 https://www.abcam.com/neuroscience/neural-markers-guide. TCGA Samples have been

8 reclassified according to the 2021 WHO CNS5 guidelines (62). Genetic information,

9 including TERT promoter mutation, EGFR amplification, and chromosome +7/−10, is

10 required to establish the molecular diagnosis of GBM. However, CGGA and NU samples

11 lack sufficient information in this regard. Consequently, classification of samples from

12 these two datasets was conducted based on the presence of IDH-mutation and/or 1p/19q

13 co-deletion.

14

15 **AS and Gene Expression Analysis in scRNA-seq Datasets**

16 ScRNA-seq data of seven IDH-WT and seven IDH-mut gliomas were downloaded from

17 European Nucleotide Archive (www.ebi.ac.uk/ena/) with dataset ID EGAS00001005472.

18 The gene expression matrix was downloaded from GEO with dataset ID GSE151506.

19 The clinical information of each sample as well as the cellular state assignment were

20 obtained from the supplementary data of previous publication (31). For AS analysis at

21 single cell resolution, the reads were aligned to the human genome reference hg19 using

22 HISAT2 and processed through MISO to estimate PSI. In pseudo-bulk strategy, the read

23 alignments from cells at the same cellular state in each patient were combined before PSI

1   estimation with MISO. We performed hierarchical clustering analysis with PSI data after

2   filtering out pseudo-bulks in which less than 50 of the 200 events were detected as well

3   as events whose PSI were detected in less than 100 pseudo-bulks. The hierarchical

4   clustering analysis were performed using Cluster v3.0 with the following setting: Similarity

5   Metric – Correlation (uncentered); Clustering method – Centroid linkage. Another

6   hierarchical clustering analysis were performed with the gene expression data of the 29

7   RBPs with the same setting in Cluster v3.0 software. Spearman's rank correlation

8   analysis was performed between RBP expression and the PSI of 108 filtered events

9   which were detected in more than 200 cells. The correlation coefficient values from each

10   RBP-event pair were used to perform hierarchical clustering analysis.

11

12   Single cell (sc) RNA-seq data of normal adult and fetal brain tissues from GSE67835 (23)

13   were downloaded from European Nucleotide Archive (www.ebi.ac.uk/ena/). Reads were

14   aligned to the human genome reference hg19 using HISAT2 and the read alignments

15   from same cell types in each sample were combined before PSI estimation with MISO.

16

17   **CRISPR-mediated Exon Skipping**

18   We selected candidates from cassettes exons that are more included in samples with

19   high AS scores to study their biological function in IDH-WT GBM/GSC cells. Eight SE or

20   MXE events in genes *TPM3*, *MPZL1*, *TJP2*, *CSNK1D*, *MARK3*, *TPM1*, *PTPRF*, and *FYN*

21   were selected by using the following criteria: (1) MeanDecreaseGini value > 0.5 or PSI

22   difference between samples with high and low AS scores > 0.2; (2) moderately or highly

23   expressed in IDH-WT GBM/GSC cells; (3) consistent splicing pattern between patient

1   tumor samples and IDH-WT GBM/GSC cells; (4) sequence around the splice sites is

2   appropriate to design CRISPR-gRNA. To induce skipping of targeted exons, CRISPR-

3   gRNAs were designed around the 5'/3' splice sites or predicted branch point

4   (http://nsclbio.jbnu.ac.kr/tools/RNABP/) of targeted exons, based on two criteria: (1)

5   Cas9-mediated cleavage site (3-4 nt upstream of the PAM sequence) less than 5 nt away

6   from the splice site or predicted branch point; (2) satisfy the "minimal off-target" criteria

7   provided by the SYNTHEGO online tool (design.synthego.com). The target sequences

8   are listed in Supplemental Table 7. The CRISPR backbone vector was used as the

9   negative control. GSC/GBM cell lines, NHNPs, or NHAs were infected with exon-targeting

10   CRISPR/Cas9 in a lentiviral vector. Heterogeneous cell population were used for

11   downstream experiment after validation of exon-skipping by RT-PCR.

12

13   **Generation of Genetically Engineered hiPSC Clones**

14   The iPSC clones, including WT, iPSC-T (*TP53*$^{-/-}$), iPSC-C (*CDKN2A/2B*$^{-/-}$), iPSC-PCT

15   (*PTEN*$^{-/-}$, *CDKN2A/2B*$^{-/-}$, *TERT*p$^{C228T/WT}$), were recently described (33, 63). We introduced

16   *IDH1*$^{R132H/WT}$ or/and *ATRX*$^{-/-}$ in iPSC-T and *MTAP*$^{-/-}$ and/or EGFRvIII overexpression in

17   iPSC-PCT using methods detailed below. *IDH1*-mutation was described to be an early

18   genetic event (64). Thus, in the TIA model, we introduced the *IDH1* mutation before the

19   *ATRX*-KO. On the other hand, EGFRvIII mutations can emerge as late and heterogenous

20   events in glioblastoma development (65). Therefore, in the PCTME model, we introduced

21   EGFRvIII as the final modification.

22

1 We utilized a "CRISPR-single base editing" method(66) to generate heterozygous *IDH1*

2 mutation at R132H (CGT to CAT). The guide RNA with the sequence of 5'-

3 GCAUGACGACCUAUGAUGAU-3' was cloned into pLKO5.sgRNA.EFS.GFP (Addgene,

4 #57822) (67). iPSCs were co-transfected with gRNA plasmid and pCMV-BE3 plasmid

5 (Addgene, #73021) (68) by electroporation using the Neon Transfection System

6 (Invitrogen, #MPK5000) according to the manufacturer's instructions. After two days,

7 GFP-positive cells were sorted and seeded into 96-well plates coated with matrigel at the

8 density of 1 cell/well using FACSMelody 3-Laser Sorter (BD Biosciences) in mTeSR Plus

9 medium supplemented with 10 μM Y-26732 (Stemcell Technologies) and 1 μM AG-120

10 (mutant IDH1 inhibitor). Y-26732 was removed when the medium was refreshed while

11 AG-120 (1 μM) was continuously added during the whole culture process of iPSCs with

12 *IDH1* mutation. Monoclonal cells were obtained after three weeks. Genomic DNA was

13 extracted, and sanger sequencing was performed to screen genomic mutation using the

14 primers listed in Supplemental Table 8. IDH1^{R132H} protein expression was confirmed by

15 immunoblotting (IB). AG-120 was removed one passage before the start of NPC induction.

16 Cellular D-2-Hydroxyglutarate (D-2HG) level was detected in NPCs using a D-2-

17 Hydroxyglutarate Assay Kit (Abcam, ab211070) according to the manufacturer's

18 instructions.

19

20 We applied a CRISPR/Cas9-based gene knockout method to induce *ATRX* or *MTAP*

21 knockout. The target gRNAs were designed using the SYNTHGO CRISPR Design Tool

22 for Knockouts (https://design.synthego.com) and cloned into PX459 plasmid (Addgene,

23 #62988) (69). iPSCs were transfected with PX459 plasmids with target gRNAs using

Lipofectamine 2000 according to the manufacturer's instructions. After 24 hr, the transfected cells were selected with 1 µg/mL puromycin for another three days. The survived cells were seeded into 96-well plates at the density of 1 cell/well. Monoclonal cells were obtained after two to three weeks. Genomic DNA was extracted, and sanger sequencing was performed to screen genomic mutation. IB was performed to measure the knockout at protein level.

Exogenous expression of EGFRvIII isoform was introduced using a lentiviral vector pLV-EF1a-EGFRvIII-IRES-Hyg (33). iPSCs or NPCs were infected with EGFRvIII-lentivirus packaged in transfected 293T cells and selected with 100 µg/mL hygromycin (Roche). Heterogeneous cell population were used for downstream experiment after validation of EGFRvIII expression by IB and cell cytometry analysis.

Animal Studies

Athymic mice (Ncr nu/nu) at 6 to 8 weeks of age were purchased from Taconic Farms (Germantown, NY). All experiments using animals were conducted under the Institutional Animal Care and Use Committee (IACUC)-approved protocols at Northwestern University in accordance with NIH and institutional guidelines.

For the tumorigenicity studies in intracranial xenograft models, luciferase reporter labeled GSC1478 (2×10^4 cells per mouse) or various iPSC avatar NPCs (5×10^5 cells per mouse) suspension were intracranially injected into the brain of individual athymic mice (five to six mice/group) using the following coordinates from bregma: 2.5 mm lateral, 1.5 mm

anterior, and 2.8 mm deep from the head skull. Bioluminescence imaging (BLI) was

conducted to monitor in vivo tumor growth using the SII Lago imaging system (Spectral

Instruments Imaging). For the survival analysis, mice were maintained until pathologic

symptoms developed resulting from tumor burden or 120 days post brain transplantation.

To determine the anti-tumor effect of ASOs in an intracranial xenograft model of GBM,

luciferase reporter labeled GSC1478 cell suspension (2×10^4 cells) was injected into the

brain of individual mice, using the following coordinates from bregma: 2.5 mm lateral, 1.5

mm anterior, and 2.8 mm deep from the head skull. Ten days after the GSC inoculation,

tumor formation was confirmed by BLI, and mice were randomly divided into PTBP1-ASO

and control-ASO groups (7-10 mice per group). Each mouse received sequential

intratumoral injection (twice a week until the first mouse reached endpoint) of the ASOs

(4 μg/mouse) mixed with in vivo-jetPEI reagent (Polyplus, 0.4 μl/mouse), which is a

polymer-based reagent that condenses nucleic acid into stable nanoparticles. BLI was

conducted to monitor in vivo tumor growth. For the survival analysis, mice were

maintained until pathologic symptoms developed resulting from tumor burden.

Statistics

Statistical analyses were carried out using GraphPad Prism version 9 or Microsoft Excel

2022. All experiments were performed on biological replicates and the exact sample size

(n) for each experiment was reported in the appropriate figure legends and methods.

Quantitative data are expressed as mean ± SD unless otherwise stated. For comparing

two groups, the two-tailed unpaired Student's t-test was used unless otherwise stated.

1   For comparing multiple groups, one-way ANOVA multiple comparisons with correction by

2   controlling the False Discovery Rate were used. For growth curve data, two-way ANOVA

3   with Geisser-Greenhouse correction were used. For survival curve data, Kaplan-Meier

4   analysis was performed, and log-rank test was used to compare between groups. For

5   limiting dilution assay, likelihood ratio test of single-hit model was used. Spearman

6   correlation analysis was used to examine the correlation between two factors unless

7   otherwise stated. $P < 0.05$ was considered significant.

8

9   **Study approval**

10   All experiments using animals were conducted under the Institutional Animal Care and

11   Use Committee (IACUC)-approved protocols at Northwestern University in accordance

12   with NIH and institutional guidelines. Human Subjects Research protocols were approved

13   by the Institutional Review Board at Northwestern University in accordance with

14   guidelines by Declaration of Helsinki, NIH, and institutional Ethics Committee.

15

16   **Data availability**

17   The RNA-seq data generated by this study have been deposited in the NCBI's Gene

18   Expression Omnibus database (GEO GSE212671). Values for all data points in graphs

19   are reported in the Supporting Data Values file. No custom algorithms were used in this

20   study.

21

22   Description of the experimental procedures related to Cell Lines and Cell Culture, Glioma

23   and Normal Brain Tissue Specimens, Plasmids, Differentiation of hiPSCs to Neural

24   Progenitor Cells (NPCs), 3D Organoid Model of iPSC Glioma Avatars, RNA Isolation, RT-

1   PCR, Immunoblotting and Immunoprecipitation Assay, CRISPR-mediated Gene

2   Knockout,   Doxycycline-inducible   shRNA-mediated   Gene   Knockdown,

3   Immunofluorescent and immunochemistry Assay, Flow Cytometric Detection, RNA-

4   sequencing in iPSC Models, In vitro Cell Proliferation Assays, In vitro Limiting Dilution

5   Assays, Ceramide extraction and liquid-chromatography mass spectrometry analysis,

6   Synthesis and in vitro transfection of ASOs, and other bioinformatics analyses are

7   detailed in the Supplemental Methods section.

8

AUTHOR CONTRIBUTIONS

S.-Y.C., B.H., and X.S. conceived the project. X.S. performed almost all the experiments and computational analyses, M.L. performed some of IHC experiments and analyses of splice site strength estimation and GC content estimation. M.W. performed some WB experiments during the revision process. C.Z., W.Z. performed initial computational analysis and provided advice. S.M., T.K., and F.F. established, and S.X. further developed hiPSC-derived glioma avatar models. H.S. performed lipidomic analysis of ceramides. S.H.S.W and A.H. analyzed the expression of CERS5 isoforms from CPTAC-GBM proteome dataset. C.M.H. provided clinical glioma tumor samples. C.H. provided general advice on 3D organoid models. H. S. and S. W. helped in analyzed data of lipid metabolome and CPTAC proteome. Manuscript writing – Original Draft, X.S., D.T., S.-Y.C., and B.H.; Writing – Review & Editing, X.S., D.T., S.-Y.C., B.H., T.H., A.G., R.I., M.L., X.Y., R.W., M.W., W.Z., C.M.H., and F.F.; Supervision, S.-Y.C. and B.H.; Project Administration, S.-Y.C. and B.H.; Funding Acquisition, S.-Y.C. and B.H.

8

9   **DECLARATION OF INTERESTS**

10   The authors declare no competing interests.

REFERENCES

1. Nicholson JG, and Fine HA. Diffuse Glioma Heterogeneity and Its Therapeutic Implications. *Cancer Discov.* 2021;11(3):575-90.

2. Louis DN, Perry A, Wesseling P, Brat DJ, Cree IA, Figarella-Branger D, et al. The 2021 WHO Classification of Tumors of the Central Nervous System: a summary. *Neuro Oncol.* 2021;23(8):1231-51.

3. Ceccarelli M, Barthel FP, Malta TM, Sabedot TS, Salama SR, Murray BA, et al. Molecular Profiling Reveals Biologically Discrete Subsets and Pathways of Progression in Diffuse Glioma. *Cell.* 2016;164(3):550-63.

4. Suva ML, and Tirosh I. The Glioma Stem Cell Model in the Era of Single-Cell Genomics. *Cancer Cell.* 2020;37(5):630-6.

5. Tirosh I, Venteicher AS, Hebert C, Escalante LE, Patel AP, Yizhak K, et al. Single-cell RNA-seq supports a developmental hierarchy in human oligodendroglioma. *Nature.* 2016;539(7628):309-13.

6. Venteicher AS, Tirosh I, Hebert C, Yizhak K, Neftel C, Filbin MG, et al. Decoupling genetics, lineages, and microenvironment in IDH-mutant gliomas by single-cell RNA-seq. *Science.* 2017;355(6332).

7. Neftel C, Laffy J, Filbin MG, Hara T, Shore ME, Rahme GJ, et al. An Integrative Model of Cellular States, Plasticity, and Genetics for Glioblastoma. *Cell.* 2019;178(4):835-49 e21.

8. Marasco LE, and Kornblihtt AR. The physiology of alternative splicing. *Nat Rev Mol Cell Biol.* 2023;24(4):242-54.

9. Raj B, and Blencowe BJ. Alternative Splicing in the Mammalian Nervous System: Recent Insights into Mechanisms and Functional Roles. *Neuron.* 2015;87(1):14-27.

10. Zhao L, Zhang J, Liu Z, Wang Y, Xuan S, and Zhao P. Comprehensive Characterization of Alternative mRNA Splicing Events in Glioblastoma: Implications for Prognosis, Molecular Subtypes, and Immune Microenvironment Remodeling. *Front Oncol.* 2020;10:555632.

11. Wang L, Shamardani K, Babikir H, Catalan F, Nejo T, Chang S, et al. The evolution of alternative splicing in glioblastoma under therapy. *Genome Biol.* 2021;22(1):48.

12. Siddaway R, Milos S, Vadivel AKA, Dobson THW, Swaminathan J, Ryall S, et al. Splicing is an alternate oncogenic pathway activation mechanism in glioma. *Nat Commun.* 2022;13(1):588.

13. Wang LB, Karpova A, Gritsenko MA, Kyle JE, Cao S, Li Y, et al. Proteogenomic and metabolomic characterization of human glioblastoma. *Cancer Cell.* 2021;39(4):509-28 e20.

14. Zhao Z, Zhang KN, Wang Q, Li G, Zeng F, Zhang Y, et al. Chinese Glioma Genome Atlas (CGGA): A Comprehensive Resource with Functional Genomic Data from Chinese Glioma Patients. *Genomics Proteomics Bioinformatics.* 2021;19(1):1-12.

15. Huang T, Yang Y, Song X, Wan X, Wu B, Sastry N, et al. PRMT6 methylation of RCC1 regulates mitosis, tumorigenicity, and radiation response of glioblastoma stem cells. *Mol Cell.* 2021;81(6):1276-91 e9.

16. Katz Y, Wang ET, Airoldi EM, and Burge CB. Analysis and design of RNA sequencing experiments for identifying isoform regulation. *Nat Methods.* 2010;7(12):1009-15.

17. Wang Q, Hu B, Hu X, Kim H, Squatrito M, Scarpace L, et al. Tumor Evolution of Glioma-Intrinsic Gene Expression Subtypes Associates with Immunological Changes in the Microenvironment. *Cancer Cell.* 2017;32(1):42-56 e6.

18. Breiman L. Random forests. *Mach Learn.* 2001;45(1):5-32.

19. Shen S, Park JW, Lu ZX, Lin L, Henry MD, Wu YN, et al. rMATS: robust and flexible detection of differential alternative splicing from replicate RNA-Seq data. *Proc Natl Acad Sci U S A.* 2014;111(51):E5593-601.

20. Hyung D, Kim J, Cho SY, and Park C. ASpedia: a comprehensive encyclopedia of human alternative splicing. *Nucleic Acids Res.* 2018;46(D1):D58-D63.

21. Ziller MJ, Ortega JA, Quinlan KA, Santos DP, Gu H, Martin EJ, et al. Dissecting the Functional Consequences of De Novo DNA Methylation Dynamics in Human Motor Neuron Differentiation and Physiology. *Cell Stem Cell.* 2018;22(4):559-74 e9.

22. Jessa S, Blanchet-Cohen A, Krug B, Vladoiu M, Coutelier M, Faury D, et al. Stalled developmental programs at the root of pediatric brain tumors. *Nat Genet.* 2019;51(12):1702-13.

23. Darmanis S, Sloan SA, Zhang Y, Enge M, Caneda C, Shuer LM, et al. A survey of human brain transcriptome diversity at the single cell level. *Proc Natl Acad Sci U S A.* 2015;112(23):7285-90.

24. Izaguirre DI, Zhu W, Hai T, Cheung HC, Krahe R, and Cote GJ. PTBP1-dependent regulation of USP5 alternative RNA splicing plays a role in glioblastoma tumorigenesis. *Mol Carcinog.* 2012;51(11):895-906.

25.   Christofk HR, Vander Heiden MG, Harris MH, Ramanathan A, Gerszten RE, Wei R, et al. The M2 splice isoform of pyruvate kinase is important for cancer metabolism and tumour growth. *Nature.* 2008;452(7184):230-3.

26.   Hu J, Ho AL, Yuan L, Hu B, Hua S, Hwang SS, et al. From the Cover: Neutralization of terminal differentiation in gliomagenesis. *Proc Natl Acad Sci U S A.* 2013;110(36):14520-7.

27.   Song X, Wan X, Huang T, Zeng C, Sastry N, Wu B, et al. SRSF3-Regulated RNA Alternative Splicing Promotes Glioblastoma Tumorigenicity by Affecting Multiple Cellular Processes. *Cancer Res.* 2019;79(20):5288-301.

28.   Yamaguchi F, Saya H, Bruner JM, and Morrison RS. Differential expression of two fibroblast growth factor-receptor genes is associated with malignant progression in human astrocytomas. *Proc Natl Acad Sci U S A.* 1994;91(2):484-8.

29.   Brignatz C, Paronetto MP, Opi S, Cappellari M, Audebert S, Feuillet V, et al. Alternative splicing modulates autoinhibition and SH3 accessibility in the Src kinase Fyn. *Mol Cell Biol.* 2009;29(24):6438-48.

30.   Mouneimne G, Hansen SD, Selfors LM, Petrak L, Hickey MM, Gallegos LL, et al. Differential remodeling of actin cytoskeleton architecture by profilin isoforms leads to distinct effects on cell migration and invasion. *Cancer Cell.* 2012;22(5):615-30.

31.   Chaligne R, Gaiti F, Silverbush D, Schiffman JS, Weisman HR, Kluegel L, et al. Epigenetic encoding, heritability and plasticity of glioma transcriptional cell states. *Nat Genet.* 2021;53(10):1469-79.

32.   Miki S, Koga T, McKinney AM, Parisian AD, Tadokoro T, Vadla R, et al. TERT promoter C228T mutation in neural progenitors confers growth advantage following telomere shortening in vivo. *Neuro Oncol.* 2022;24(12):2063-75.

33.   Koga T, Chaim IA, Benitez JA, Markmiller S, Parisian AD, Hevner RF, et al. Longitudinal assessment of tumor development using cancer avatars derived from genetically engineered pluripotent stem cells. *Nat Commun.* 2020;11(1):550.

34.   Sundar SJ, Shakya S, Barnett A, Wallace LC, Jeon H, Sloan A, et al. Three-dimensional organoid culture unveils resistance to clinical therapies in adult and pediatric glioblastoma. *Transl Oncol.* 2022;15(1):101251.

35.   Levy M, and Futerman AH. Mammalian ceramide synthases. *IUBMB Life.* 2010;62(5):347-56.

36.   Grosch S, Schiffmann S, and Geisslinger G. Chain length-specific properties of ceramides. *Prog Lipid Res.* 2012;51(1):50-62.

37.   Sassa T, Hirayama T, and Kihara A. Enzyme Activities of the Ceramide Synthases CERS2-6 Are Regulated by Phosphorylation in the C-terminal Region. *J Biol Chem.* 2016;291(14):7477-87.

38.   Zhao ZJ, and Zhao R. Purification and cloning of PZR, a binding protein and putative physiological substrate of tyrosine phosphatase SHP-2. *J Biol Chem.* 1998;273(45):29367-72.

39.   Chen D, Cao L, and Wang X. MPZL1 promotes tumor cell proliferation and migration via activation of Src kinase in ovarian cancer. *Oncol Rep.* 2019;42(2):679-87.

40.   Feng J, Ouyang H, Wang J, Pan D, Sheng L, Xu C, et al. MPZL1 upregulation promotes tumor metastasis and correlates with unfavorable prognosis in non-small cell lung cancer. *Carcinogenesis.* 2022;43(10):919-29.

41.   Zhao R, and Zhao ZJ. Dissecting the interaction of SHP-2 with PZR, an immunoglobulin family protein containing immunoreceptor tyrosine-based inhibitory motifs. *J Biol Chem.* 2000;275(8):5453-9.

42.   Zhang J, Zhang F, and Niu R. Functions of Shp2 in cancer. *J Cell Mol Med.* 2015;19(9):2075-83.

43.   Consortium EP. An integrated encyclopedia of DNA elements in the human genome. *Nature.* 2012;489(7414):57-74.

44.   Damianov A, Ying Y, Lin CH, Lee JA, Tran D, Vashisht AA, et al. Rbfox Proteins Regulate Splicing as Part of a Large Multiprotein Complex LASR. *Cell.* 2016;165(3):606-19.

45.   Qian H, Kang X, Hu J, Zhang D, Liang Z, Meng F, et al. Reversing a model of Parkinson's disease with in situ converted nigral neurons. *Nature.* 2020;582(7813):550-6.

46.   Li Y, Ren Z, Peng Y, Li K, Wang X, Huang G, et al. Classification of glioma based on prognostic alternative splicing. *BMC Med Genomics.* 2019;12(1):165.

47.   Zeng Y, Zhang P, Wang X, Wang K, Zhou M, Long H, et al. Identification of Prognostic Signatures of Alternative Splicing in Glioma. *J Mol Neurosci.* 2020;70(10):1484-92.

48.   Kim JH, Jeong K, Li J, Murphy JM, Vukadin L, Stone JK, et al. SON drives oncogenic RNA splicing in glioblastoma by regulating PTBP1/PTBP2 switching and RBFOX2 activity. *Nat Commun.* 2021;12(1):5551.

49.   Zhou X, Wang R, Li X, Yu L, Hua D, Sun C, et al. Splicing factor SRSF1 promotes gliomagenesis via oncogenic splice-switching of MYO1B. *J Clin Invest.* 2019;129(2):676-93.

50. Kim HJ, Park JW, and Lee JH. Genetic Architectures and Cell-of-Origin in Glioblastoma. *Front Oncol.* 2020;10:615400.

51. Robson JP, Wagner B, Glitzner E, Heppner FL, Steinkellner T, Khan D, et al. Impaired neural stem cell expansion and hypersensitivity to epileptic seizures in mice lacking the EGFR in the brain. *FEBS J.* 2018;285(17):3175-96.

52. Ayuso-Sacido A, Moliterno JA, Kratovac S, Kapoor GS, O'Rourke DM, Holland EC, et al. Activated EGFR signaling increases proliferation, survival, and migration and blocks neuronal differentiation in post-natal neural stem cells. *J Neurooncol.* 2010;97(3):323-37.

53. Figueroa ME, Abdel-Wahab O, Lu C, Ward PS, Patel J, Shih A, et al. Leukemic IDH1 and IDH2 mutations result in a hypermethylation phenotype, disrupt TET2 function, and impair hematopoietic differentiation. *Cancer Cell.* 2010;18(6):553-67.

54. Lu C, Ward PS, Kapoor GS, Rohle D, Turcan S, Abdel-Wahab O, et al. IDH mutation impairs histone demethylation and results in a block to cell differentiation. *Nature.* 2012;483(7390):474-8.

55. Modrek AS, Golub D, Khan T, Bready D, Prado J, Bowman C, et al. Low-Grade Astrocytoma Mutations in IDH1, P53, and ATRX Cooperate to Block Differentiation of Human Neural Stem Cells via Repression of SOX2. *Cell Rep.* 2017;21(5):1267-80.

56. Rosiak K, Smolarz M, Stec WJ, Peciak J, Grzela D, Winiecka-Klimek M, et al. IDH1R132H in Neural Stem Cells: Differentiation Impaired by Increased Apoptosis. *PLoS One.* 2016;11(5):e0154726.

57. Mendel M, Delaney K, Pandey RR, Chen KM, Wenda JM, Vagbo CB, et al. Splice site m(6)A methylation prevents binding of U2AF35 to inhibit RNA splicing. *Cell.* 2021;184(12):3125-42 e25.

58. Zhou Z, and Fu XD. Regulation of splicing by SR proteins and SR protein-specific kinases. *Chromosoma.* 2013;122(3):191-207.

59. Wang K, Pan S, Zhao P, Liu L, Chen Z, Bao H, et al. PTBP1 knockdown promotes neural differentiation of glioblastoma cells through UNC5B receptor. *Theranostics.* 2022;12(8):3847-61.

60. De Silva MI, Stringer BW, and Bardy C. Neuronal and tumourigenic boundaries of glioblastoma plasticity. *Trends Cancer.* 2023;9(3):223-36.

61. Kim D, Langmead B, and Salzberg SL. HISAT: a fast spliced aligner with low memory requirements. *Nat Methods.* 2015;12(4):357-60.

62. Zakharova G, Efimov V, Raevskiy M, Rumiantsev P, Gudkov A, Belogurova-Ovchinnikova O, et al. Reclassification of TCGA Diffuse Glioma Profiles Linked to

Transcriptomic, Epigenetic, Genomic and Clinical Data, According to the 2021 WHO CNS Tumor Classification. *Int J Mol Sci.* 2022;24(1).

63. Miki S, Koga T, McKinney AM, Parisian AD, Tadokoro T, Vadla R, et al. TERT promoter C228T mutation in neural progenitors confers growth advantage following telomere shortening in vivo. *Neuro Oncol.* 2022.

64. Watanabe T, Nobusawa S, Kleihues P, and Ohgaki H. IDH1 mutations are early events in the development of astrocytomas and oligodendrogliomas. *Am J Pathol.* 2009;174(4):1149-53.

65. Eskilsson E, Rosland GV, Talasila KM, Knappskog S, Keunen O, Sottoriva A, et al. EGFRvIII mutations can emerge as late and heterogenous events in glioblastoma development and promote angiogenesis through Src activation. *Neuro Oncol.* 2016;18(12):1644-55.

66. Wei S, Wang J, Oyinlade O, Ma D, Wang S, Kratz L, et al. Heterozygous IDH1(R132H/WT) created by "single base editing" inhibits human astroglial cell growth by downregulating YAP. *Oncogene.* 2018;37(38):5160-74.

67. Heckl D, Kowalczyk MS, Yudovich D, Belizaire R, Puram RV, McConkey ME, et al. Generation of mouse models of myeloid malignancy with combinatorial genetic lesions using CRISPR-Cas9 genome editing. *Nat Biotechnol.* 2014;32(9):941-6.

68. Komor AC, Kim YB, Packer MS, Zuris JA, and Liu DR. Programmable editing of a target base in genomic DNA without double-stranded DNA cleavage. *Nature.* 2016;533(7603):420-4.

69. Ran FA, Hsu PD, Wright J, Agarwala V, Scott DA, and Zhang F. Genome engineering using the CRISPR-Cas9 system. *Nat Protoc.* 2013;8(11):2281-308.
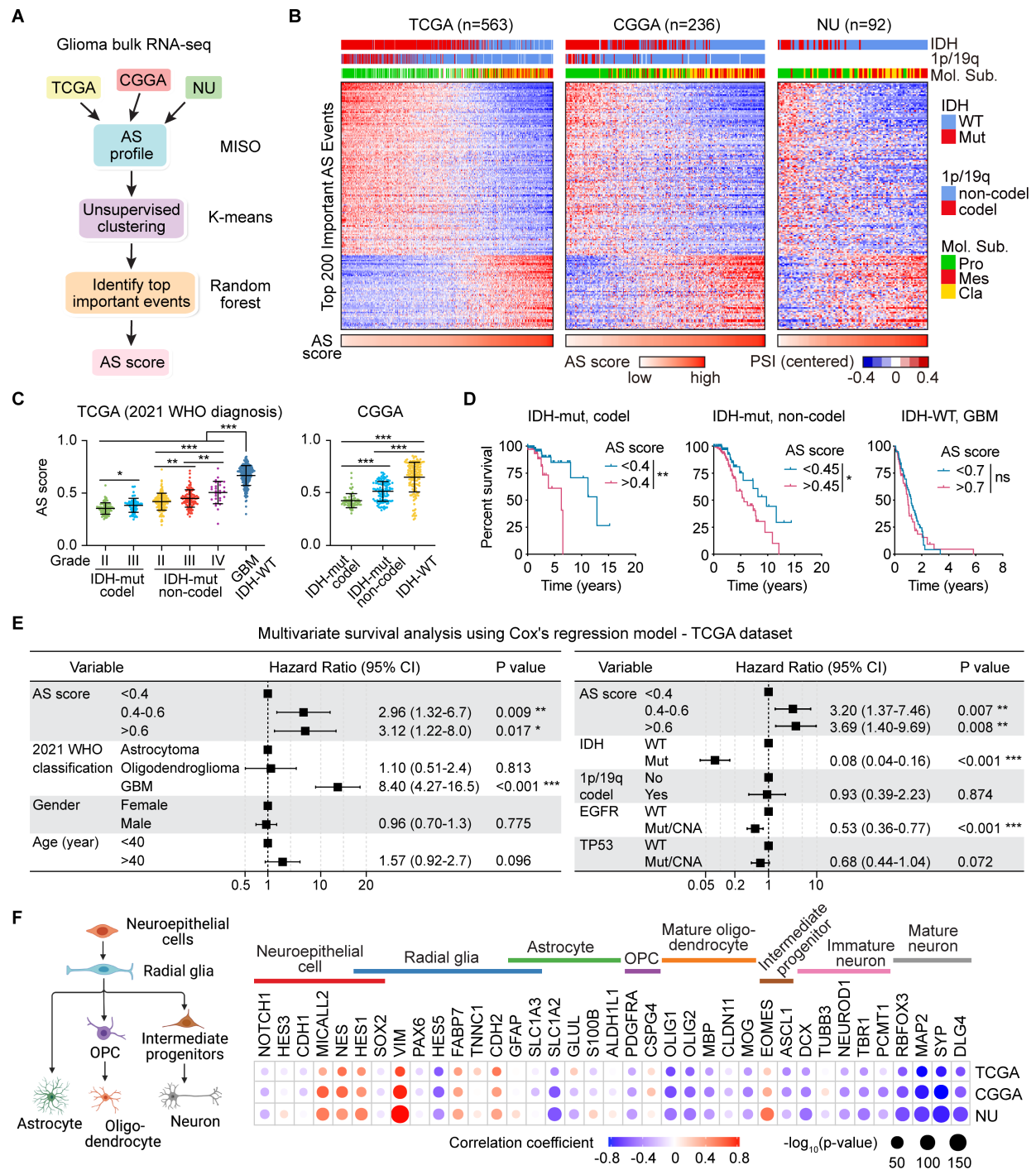
Figure 1: Unsupervised splicing analysis in bulk gliomas reveals a prognostic AS signature linked to neural lineage differentiation.

(A) Computational pipeline of AS analysis in gliomas. **(B)** Heatmaps showing the PSI values of the 200 AS events across three glioma samples. Samples were ordered based on their AS scores. Annotations on top show the association of AS landscape with *IDH* mutation, 1p/19q co-deletion, and predefined molecular subtyping. Pro, proneural; Mes, mesenchymal; Cla, classical; Mut, mutant; WT, wildtype. **(C)** AS scores of glioma samples in indicated groups from TCGA and CGGA datasets, analyzed using one-way ANOVA multiple comparisons with correction by controlling the False Discovery Rate. **(D)** Kaplan-Meier analyses in TCGA gliomas grouped by AS score. Log-rank test was used to compare between groups. **(E)** Multivariate cox regression analysis for overall survival in TCGA glioma samples. HR: hazard ratio; CI: confidence interval. **(F)** The correlation between AS score and the expression of neural lineage markers. Dot sizes indicate the p-value from spearman correlation analysis, and colors indicate correlation coefficient value. The cartoon on left shows the neural differentiation trajectory. *, p<0.05; **, p<0.01; ***, p<0.001; ns, not significant.
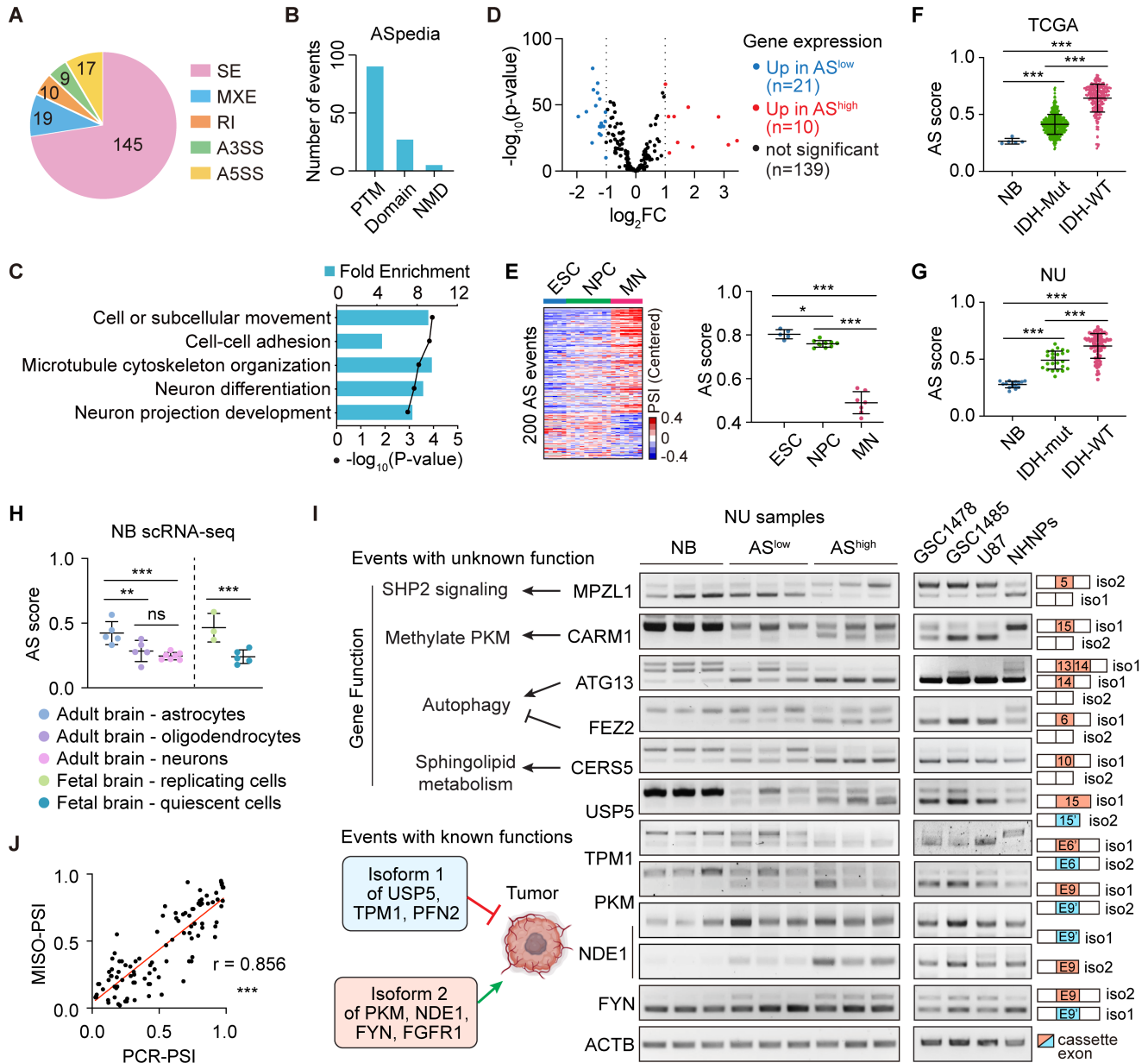
Figure 2: An overview of the 200 events and validation of their AS pattern.
(A) Distribution of the 200 AS events in each category: SE, skipped exons; MXE, mutually exclusive exons; A5SS/A3SS, alternative 5'/3' splice sites; RI, retained introns. **(B)** Functional impact of 200 AS events annotated by the ASpedia database. PTM, posttranslational modification; NMD, nonsense-mediated decay. **(C)** Top 5 significantly enriched GO biological processes of the 170 genes. **(D)** Volcano plot for the differential expression of 170 AS-affected genes between samples with high and low AS scores from TCGA dataset. **(E)** AS profiling in human embryonic stem cell (ESC)-derived neuronal differentiation model. Left, Heatmaps show the AS landscape of 200 events in ESC, differentiated neural progenitor cells (NPC) and motor neurons (MN). Right, AS scores in indicated groups. **(F-G)** AS scores in normal brains (NB), IDH-mut, and IDH-WT gliomas from TCGA (**F**) and NU (**G**) datasets. **(H)** AS scores in indicated cell types from scRNA-seq data of adult and fetal brains. **(I)** RT-PCR analysis with isoform-specific primers for indicated genes in normal brains (NB), NU glioma tissues (AS^{low} and AS^{high}), GSC/GBM cell lines, and normal human neural progenitors (NHNPs). **(J)** Pearson correlation analysis between MISO-estimated PSI and RT-PCR quantified PSI. Data were analyzed using one-way ANOVA multiple comparisons with correction by controlling the False Discovery Rate in E-H. *, p<0.05; **, p<0.01; ***, p<0.001; ns, not significant.
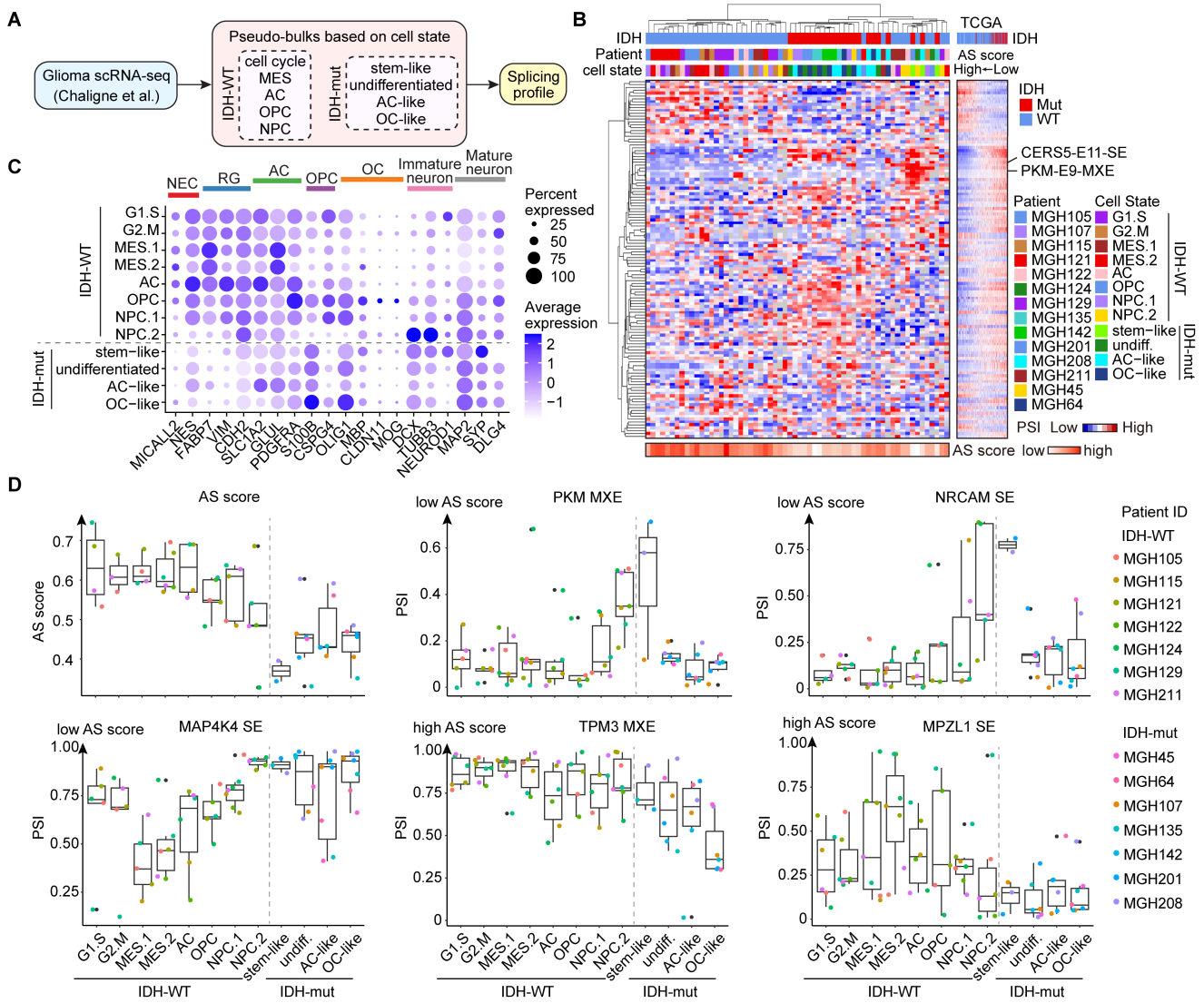
Figure 3: Intra-tumoral AS heterogeneity is associated with the developmental hierarchy in glioma.
(A) Computational pipeline of AS analysis using a cell-state based pseudo-bulk strategy in scRNA-seq data of gliomas. **(B)** Hierarchical clustering analysis with the PSI data of events in pseudo-bulks. The heatmap on the right illustrates the PSI data of events at the same order in TCGA samples. **(C)** Expression of neural lineage markers in each cell state. Dot sizes indicate the percentage of cells in each group expressing the gene, and colors indicate average expression levels. NEC, neuroepithelial cells; RG, radial glia; AC, astrocyte; OPC, oligodendrocyte progenitors; OC, oligodendrocytes. **(D)** Box-plots showing the AS score and PSI distribution of representative AS events in each cell states. The box representing the interquartile range of the data, the line within the box representing the median, and the whiskers extending to the most extreme data points within 1.5 times the interquartile range. Individual data points beyond this range are shown as dots. The color of the dots represents the patient.
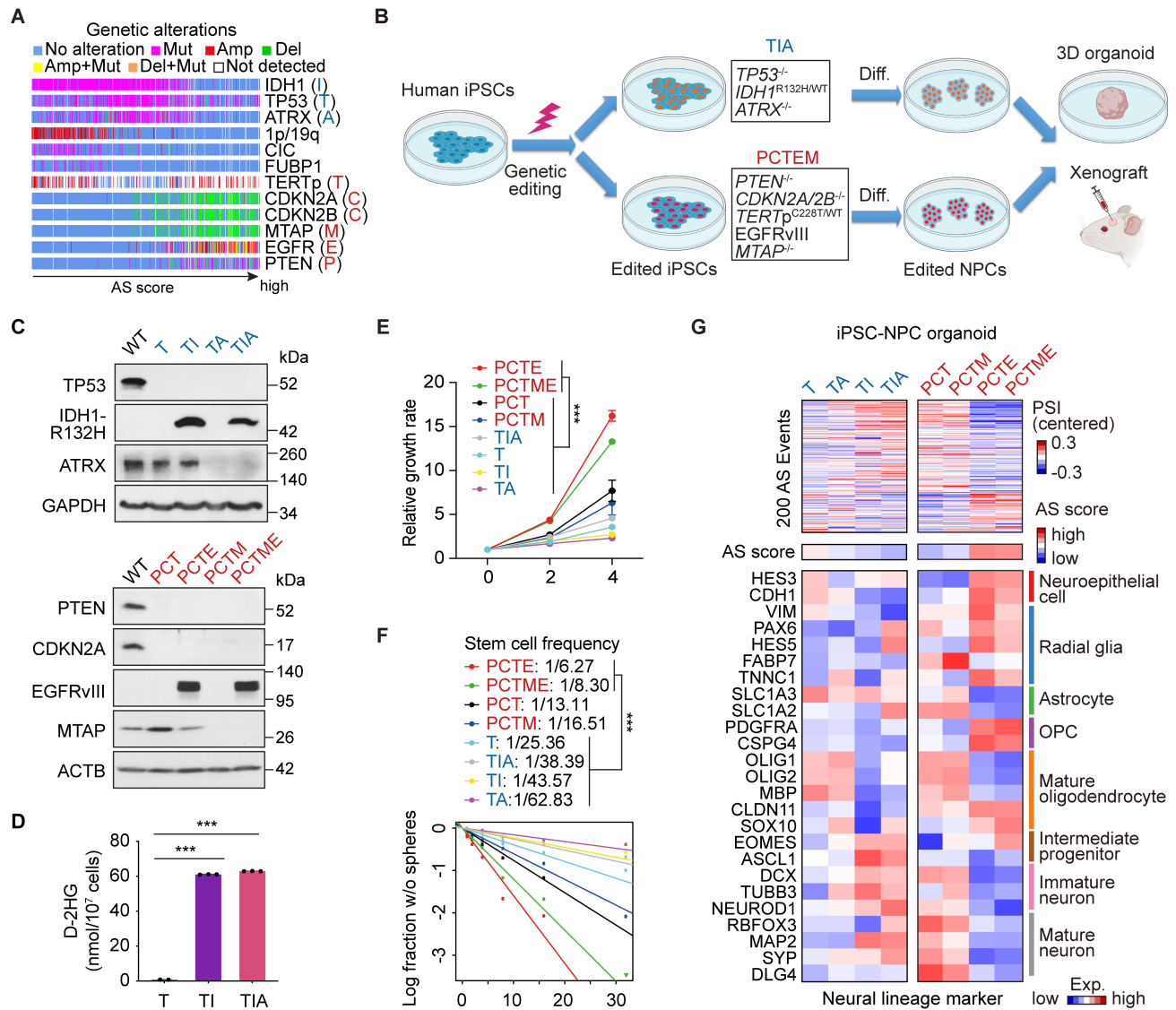
Figure 4: Glioma driver mutations modulate AS landscape and neural developmental programs in iPSC-based glioma models.
**(A)** Mutational landscape of frequent somatic alterations in TCGA glioma samples ordered by AS score. **(B)** Workflow of iPSC editing, NPC induction, and in vitro and in vivo model system. **(C)** IB for edited iPSCs. WT, wild type; T, *TP53*^{-/-}; TI, T+*IDH1*[R132H/WT]; TA, T+*ATRX*^{-/-}; TIA, TI+*ATRX*^{-/-}; PCT, *PTEN*^{-/-} *CDKN2A/2B*[-/-], *TERT*p[-/-]; PCTE, PCT+EGFRvIII-OE; PCTM, PCT+*MTAP*^{-/-}; PCTME, PCTM+EGFRvIII-OE. **(D)** Detection of intracellular D-2HG in edited NPCs. N = 2-3. **(E-F)** Cell proliferation (**E**, N = 3-6) and self-renewal ability (**F**) of edited NPCs. **(G)** Heatmap showing the AS landscapes and the expression of neural lineage markers in iPSC organoids harboring indicated mutations. Data were analyzed using two-tailed unpaired t-test in D, two-way ANOVA in E, and likelihood ratio test of single-hit model in F. ***, p<0.001.
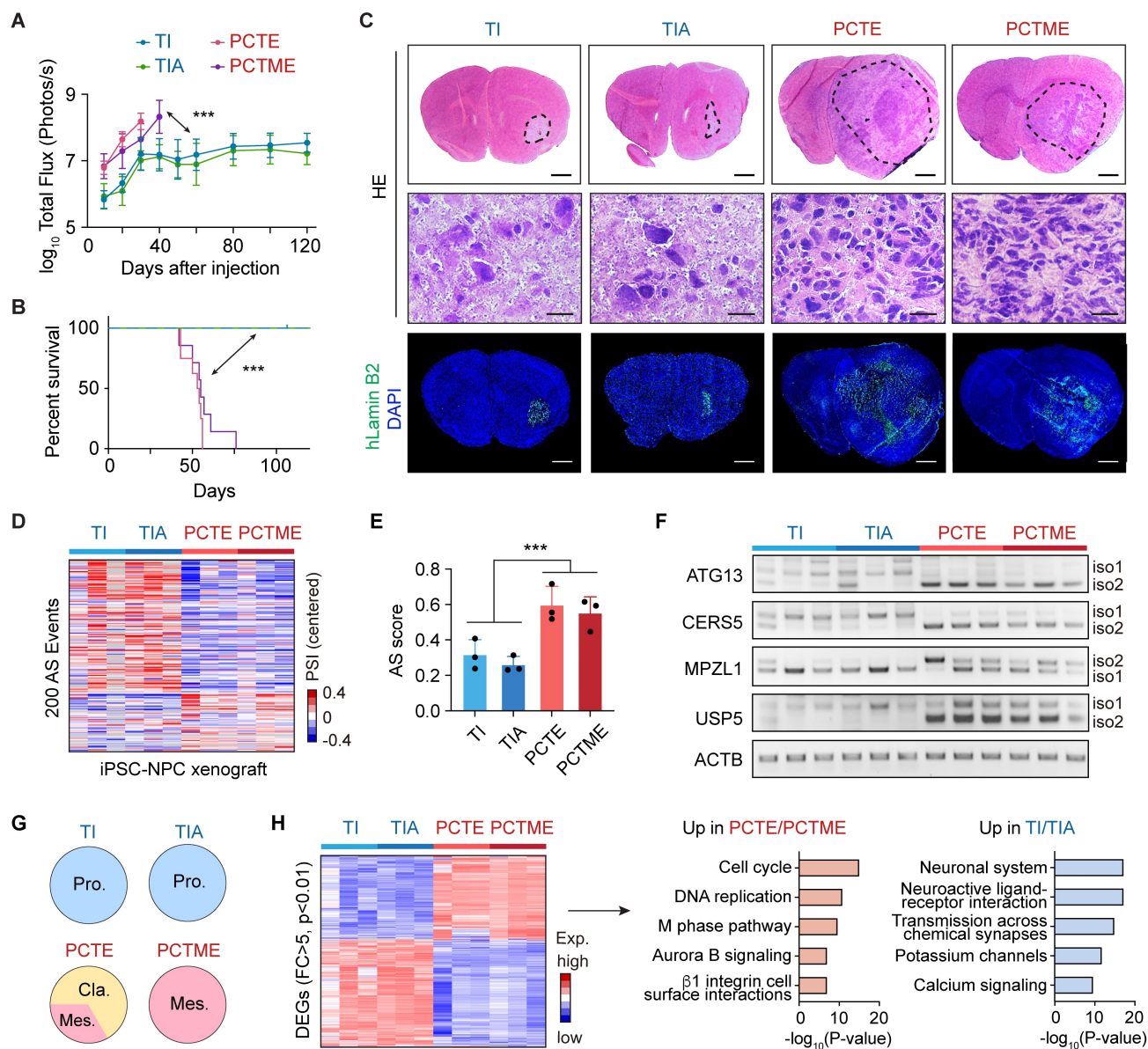
Figure 5: In vivo glioma models from edited iPSCs recapitulate the gene expression and AS signatures of clinical gliomas.

(A) Quantification of bioluminescent intensity emitted from indicated intracranial xenografts. N = 5-6. **(B)** Kaplan-Meier analysis of tumor-bearing mice. Log-rank test was used to compare between groups. N = 5-8. **(C)** Representative images of H&E (upper and middle) and IF (lower) staining with a human-specific anti-laminin B2 antibody on brain sections from tumor-bearing mice (N = 5-6). Scale bars, upper and lower panel, 1 mm; middle panel, 20 μm. **(D-E)** AS landscape of the 200 events (**D**) and AS scores (**E**) in iPSC xenografts harboring indicated mutations from RNA-seq data. **(F)** RT-PCR analysis with human-specific primers in intracranial xenografts from edited NPCs. **(G)** Subtyping results of iPSC-derived glioma xenografts based on a previously reported molecular subtype signatures using GlioVis subtyping tools. N = 3. **(H)** Left, Heatmap showing the differentially expressed genes between TI/TIA and PCTE/PCTME xenografts. Right, Top 5 significantly enriched GO biological processes of the differentially expressed genes between TI/TIA and PCTE/PCTME xenografts. Data were analyzed using two-way ANOVA in A, log-rank test in B, and two-tailed unpaired t-test in E. ***, p<0.001.
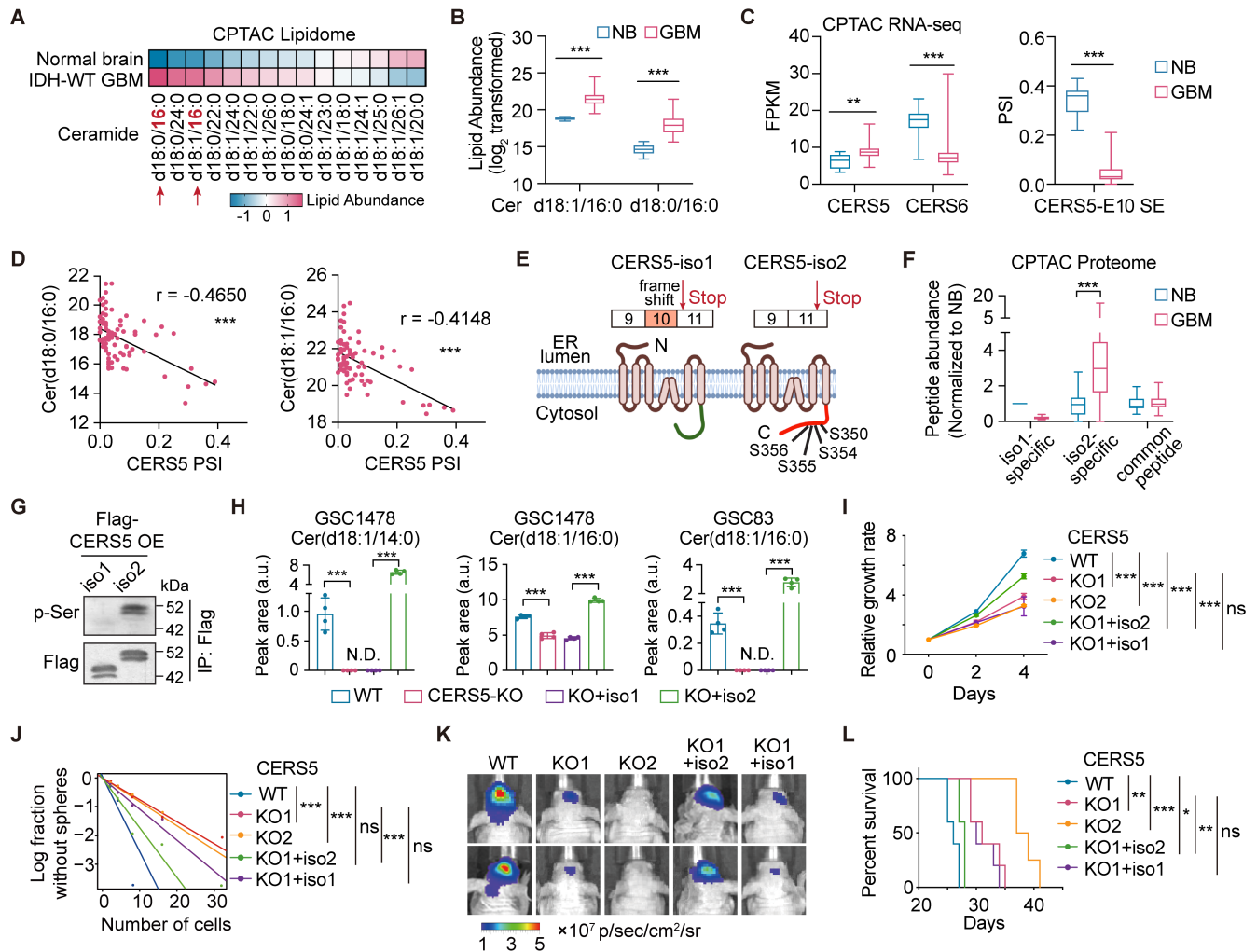
Figure 6: AS of CERS5-E10 affects the ceramide component and oncogenic potential of glioma cells.
(A-B) Ceramide abundance between normal brain and GBM. "d18" represents a sphingoid base with 18 carbons. The number after ":" indicates the presence of double bonds, and the number after "/" denotes the carbon length in the fatty acid chain. **(C)** Gene expression of *CERS5*, *CERS6* (left) and PSI of *CERS5*-E10-SE between normal brain and GBM. **(D)** Spearman correlation analysis between C16-ceramide and PSI of *CERS5*-E10-SE. **(E)** A cartoon showing CERS5 isoforms. **(F)** Abundance of CERS5 peptides analyzed from CPTAC-proteome data. **(G)** IP-IB in GSC46 overexpressed with CERS5 isoforms. **(H)** Lipid-MS analysis of ceramides abundance in GSCs. N = 4. N.D., not detected. **(I-L)** Effects of CERS5-KO and rescue on proliferation (**I**, N = 3-6), sphere-formation (**J**), xenograft growth of GSC1478 (**K**, representative BLI at 18 days after inoculation) and mice survival (**L**, N = 4-5). Data were analyzed using two-tailed unpaired t-test in B, C, F, and H, two-way ANOVA in, likelihood ratio test in J, and log-rank test in L. In B, C, and F, the box represents the interquartile range, the line within the box represents the median, and the whiskers extending to the maximum and minimum values. *, p<0.05; **, p<0.01; ***, p<0.001; ns, not significant.
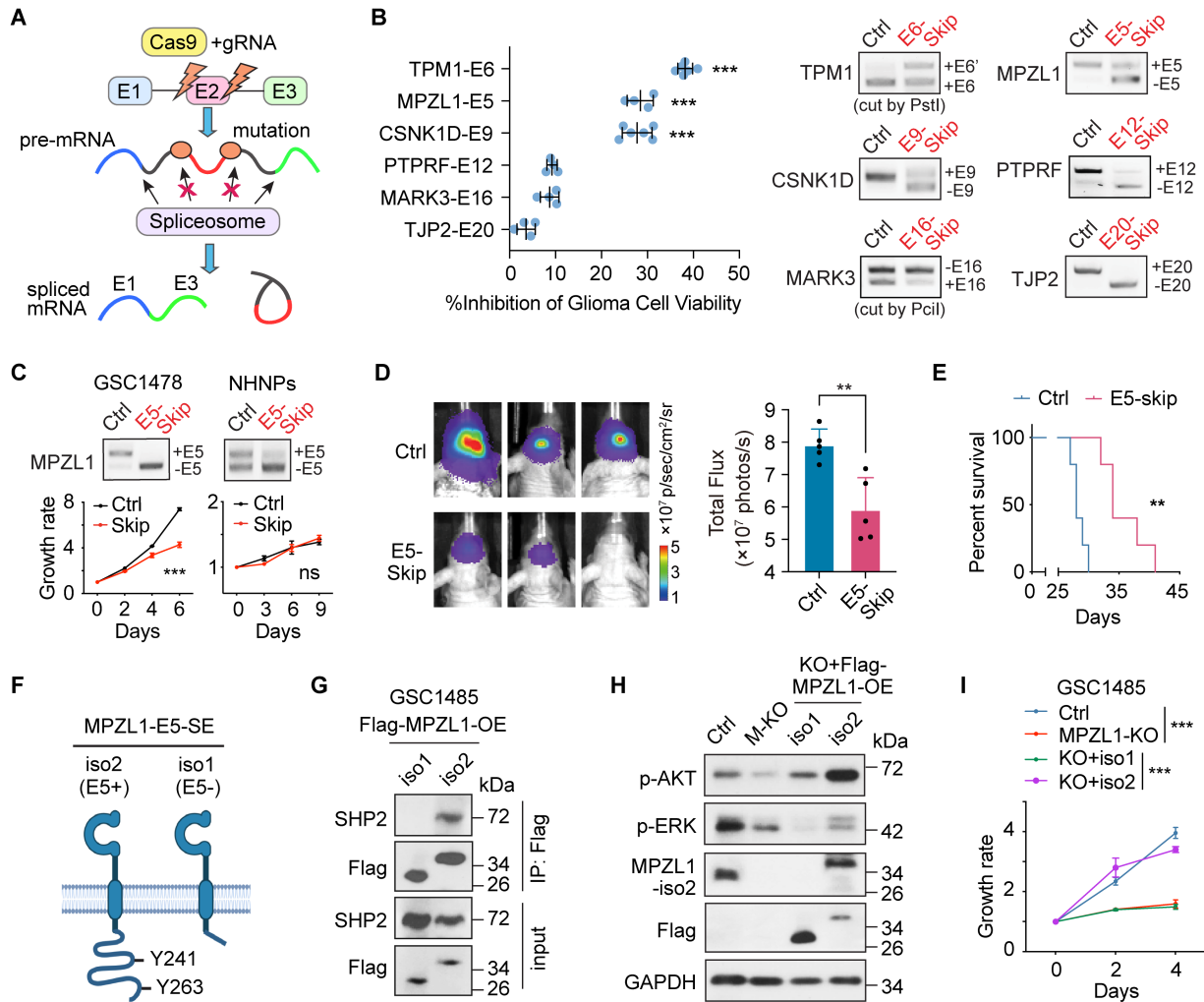
Figure 7: Modulation of MPZL1 splicing impacts its interaction with SHP2 and the subsequent oncogenic signaling in glioma cells.
(A) Scheme showing CRISPR-based splicing modulation. **(B)** Left, effects on cell viability of GSC1485 by skipping of indicated exons. Right, RT-PCR. N = 4-6. **(C)** Effect of *MPZL1*-E5 skipping on the proliferation of indicated cells. Upper, RT-PCR. Lower, growth curve. N = 4. **(D-E)** Effects of *MPZL1*-E5 skipping on xenograft growth of GSC1478 (**D**, representative BLI and quantification, N = 5) and mouse survival (**E**, N = 5). **(F)**, A cartoon showing MPZL1 isoforms. **(G)** IP-IB in GSC1485 overexpressed with MPZL1 isoforms. **(H-I)** Effects of MPZL1-KO and rescue on signaling pathways (**H**) and proliferation (**I**, N = 3-4) of GSC1485. Data were analyzed using two-tailed unpaired t-test in B and D, two-way ANOVA in C and I, and log-rank test in E. **, p<0.01; ***, p<0.001; ns, not significant.
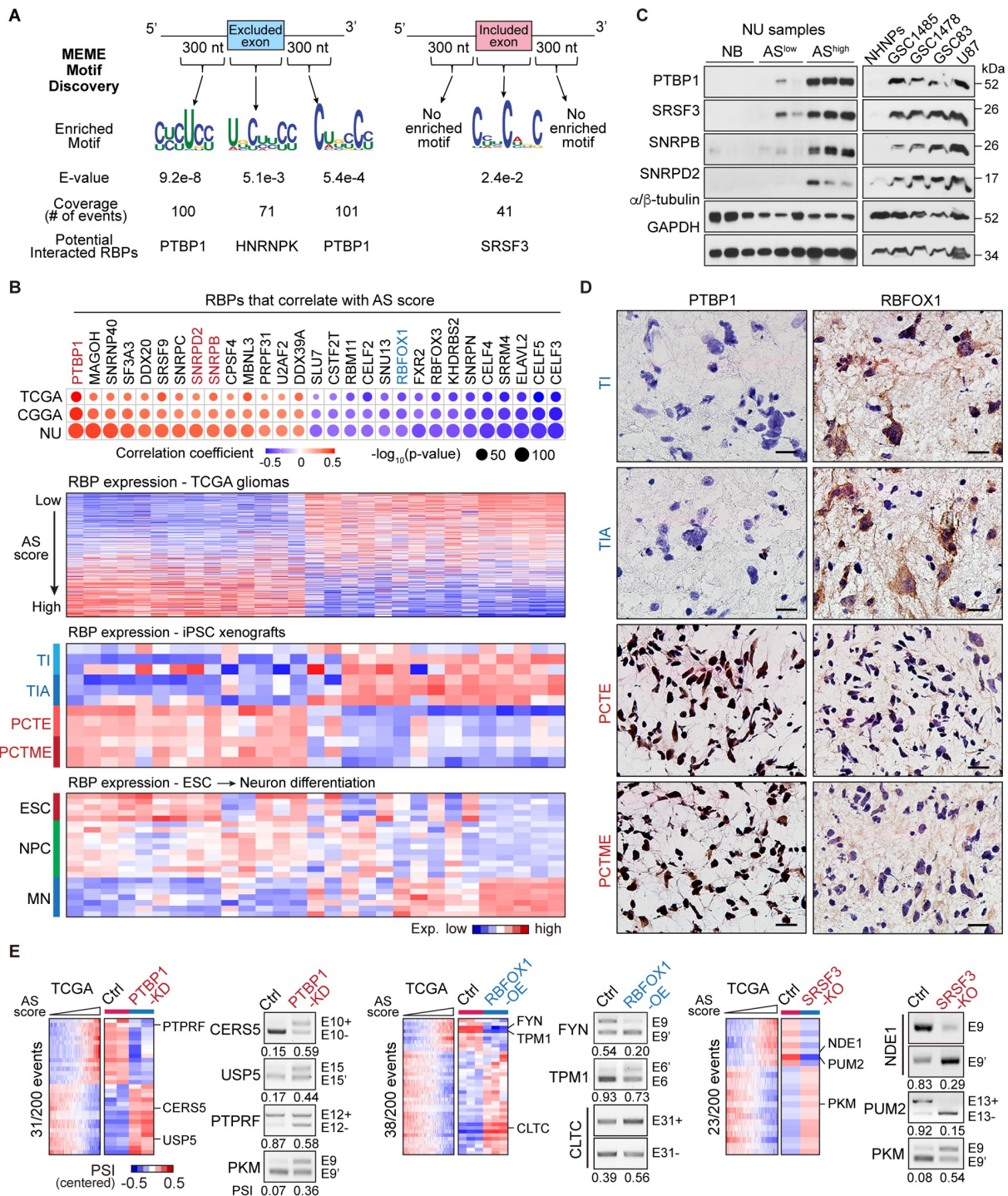
Figure 8: A group of RBPs modulate the AS landscape in glioma.
(A) Motif analysis around the splice sites of the exons from the 200 events and predicted binding RBPs. **(B)** Upper, dot plot showing the correlation between AS score and the expression of each RBPs. Dot sizes indicate the p-value from spearman correlation analysis, and colors indicate correlation coefficient value. Bottom, heatmap showing the expression of each RBPs in TCGA gliomas, iPSC glioma xenografts, and human ESC to MN differentiation model. **(C)** IB analysis of indicated RBPs in normal brains (NB), NU glioma tissues with low or high AS scores (AS^low and AS^high), and indicated cell lines. **(D)** IHC staining shows the expression of PTBP1 and RBFOX1 in iPSC glioma xenografts. Scale bars, 20 μm. **(E)** Heatmaps show the PSI distribution of the events that are from the 200 events and affected by PTBP1-KD, RBFOX1-OE, or SRSF3-KO. RT-PCR shows the validation of AS changes in GSC1485 with indicated treatment. The numbers below the PCR plots show the PCR-quantified PSI values.
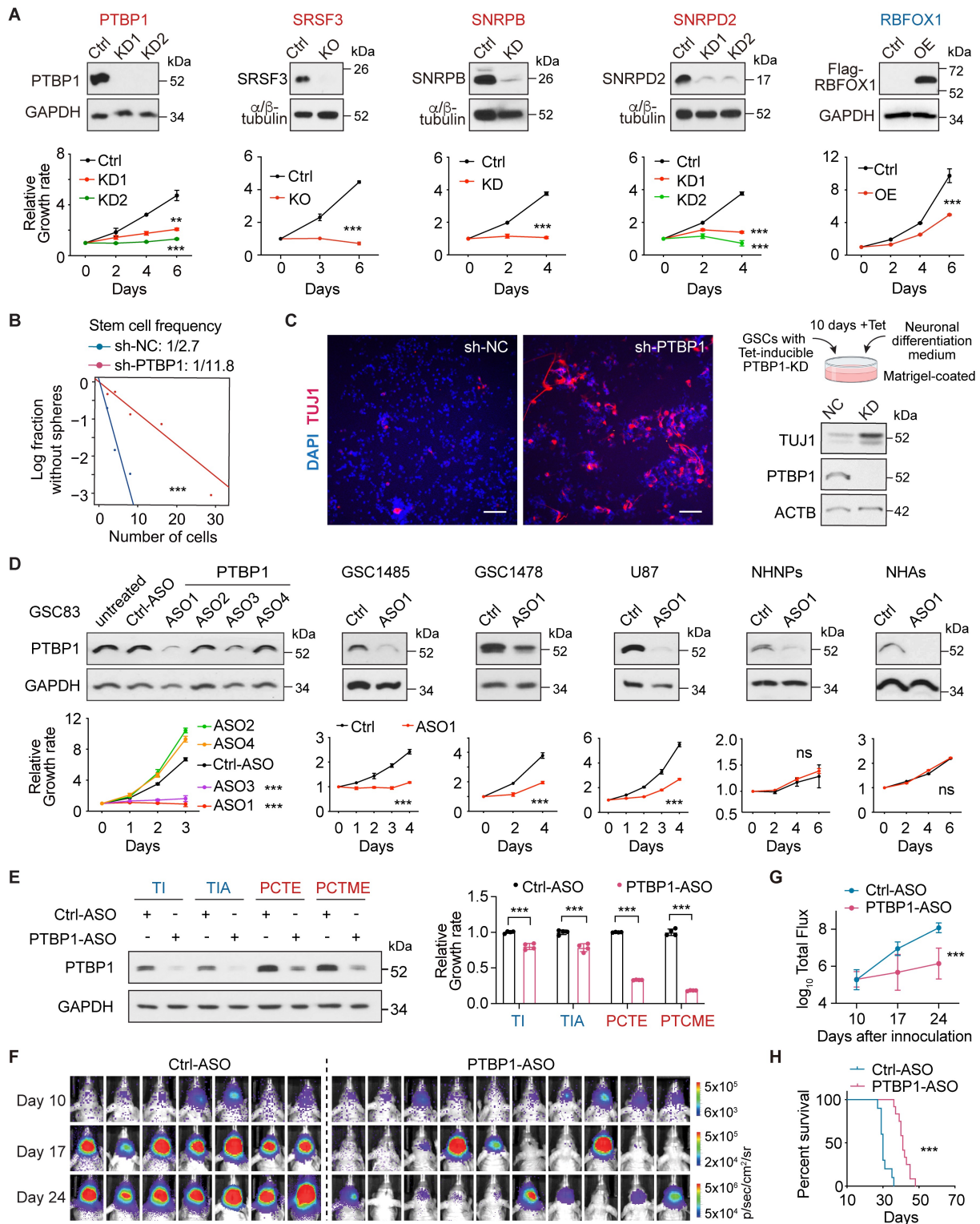
Figure 9: Targeting PTBP1 inhibited cell growth and induced neuronal-like differentiation in GSCs.
(A) Effect of overexpression (OE), knockdown (KD) or knockout (KO) of indicated RBPs on cell proliferation of GSC1485 (PTBP1, SRSF3, SNRPB, SNRPD2) or GSC1478 (RBFOX1). Upper, IB. Lower, cell proliferation curve. N = 2-4. **(B)** Sphere-formation analysis in GSC1478 treated with shRNA-PTBP1 (sh-PTBP1) or a negative control (sh-NC). **(C)** IF and IB analysis of TUJ1 in GSC1478 cells treated with sh-PTBP1 or sh-NC. Scale bars, 100 μm. **(D)** Effects of PTBP1-targeting ASOs on PTBP1 expression (IB, upper) and cell proliferation (lower) in indicated cells. N = 3-6. **(E)** Effects of PTBP1-targeting ASO1 on PTBP1 expression (IB, left) and cell proliferation (right) in edited iPSC-derived NPCs with indicated mutations. N = 4. **(F-H)** In vivo effects of PTBP1-ASO1 on the growth of GSC1478-derived intracranial xenografts (**F**, BLI images of brain glioma xenografts. **G**, quantification) and survival of mice (**H**). N = 7-10. Data were analyzed using two-way ANOVA in A, D, and G, two-tailed unpaired t-test in E, likelihood ratio test in B, and log-rank test in H. **, p<0.01; ***, p<0.001; ns, not significant.